

# Multi-Objective Hierarchical Optimization with Large Language Models

Andrey Schwanke<sup>1</sup>, Lyubomir Ivanov<sup>1</sup>, David Salinas<sup>2</sup>, Frank Hutter<sup>3,2,1</sup> and Arber Zela<sup>2</sup>

<sup>1</sup>University of Freiburg, Germany

<sup>2</sup>ELLIS Institute Tübingen, Germany

<sup>3</sup>Prior Labs

andrejschwanke19@gmail.com arber.zela@tue.ellis.eu

## Abstract

Despite their widespread adoption in various domains, especially due to their powerful reasoning capabilities, Large Language Models (LLMs) are not the off-the-shelf choice to drive multi-objective optimization yet. Conventional strategies rank high in benchmarks due to their intrinsic capabilities to handle numerical inputs and careful modelling choices that balance exploration and Pareto-front exploitation, as well as handle multiple (conflicting) objectives. In this paper, we close this gap by leveraging LLMs as surrogate models and candidate samplers inside a structured hierarchical search strategy. By adaptively partitioning the input space into disjoint hyperrectangular regions and ranking them with a composite score function, we restrict the generative process of the LLM to specific, high-potential sub-spaces, hence making the problem easier to solve as the LLM doesn't have to reason about the global structure of the problem, but only locally instead. We show that under standard regularity assumptions, our algorithm generates candidate solutions that converge to the true Pareto set in Hausdorff distance. Empirically, it consistently outperforms the global LLM-based multi-objective optimizer and is on par with standard evolutionary and Bayesian optimization algorithm on synthetic and real-world benchmarks.

## 1 Introduction

Optimizing multiple unknown functions with potentially conflicting objectives remains a challenging yet important problem arising in many areas [Chinchuluun and Pardalos, 2007; Coello Coello, 1999], including machine learning [Sener and Koltun, 2018], engineering [Marler and Arora, 2004], material science [Gopakumar *et al.*, 2018] and robotics [Tesch *et al.*, 2013]. For such multi-objective optimization (MOO) problems, finding a single solution that optimizes all objectives simultaneously is typically impossible, hence, we are interested in a set of Pareto optimal solutions [Deb, 2001].

In practice, for many MOO problems, we do not have access to gradient information and at least one of the objectives is expensive to evaluate [Jones *et al.*, 1998]. For

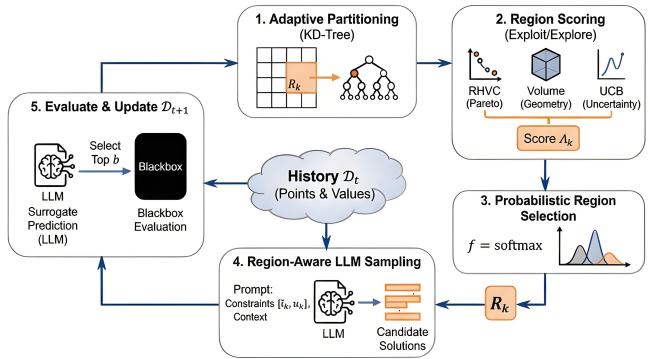


Figure 1: Illustration of MOHOLLM’s optimization pipeline.

example, synthesizing molecules often requires costly wet-lab experiments or computationally expensive simulations, requiring days or potentially weeks for obtaining a single function evaluation [Shields *et al.*, 2021]. Classical approaches such as Multi-Objective Evolutionary Algorithms (MOEAs) [Deb, 2001; Deb *et al.*, 2002; Deb and Jain, 2014] and Bayesian Optimization (MOBO) [Daulton *et al.*, 2021; Daulton *et al.*, 2022] are standard and effective choices. However, they typically require assumptions on function properties and lack mechanisms to directly integrate domain knowledge into the optimization process.

In the past few years, Large Language Models (LLMs) [Touvron and others, 2023; OpenAI, 2023] and their in-context learning (ICL) capabilities [Brown *et al.*, 2020; Krishnamurthy *et al.*, 2024] have created substantial advancements across various fields. More recently, we have seen an adoption of LLMs in optimization too [Liu *et al.*, 2024; Agarwal *et al.*, 2025; Zhang *et al.*, 2023; Yang *et al.*, 2024], where LLMs are used to guide the search by generating candidate solutions by encoding task information and specifications inside prompts. However, recent findings suggest that such LLM-based optimizers may exhibit high sampling bias and sensitivity to prompt design [Liu *et al.*, 2024; Schwanke *et al.*, 2025]. Moreover, their extension to MOO involves additional complexities arising from the necessity to balance the multiple objectives.

In this paper, we introduce **MOHOLLM** (Multi-Objective Hierarchical Optimization with LLMs), a framework that mitigates these issues through adaptive search space par-

titioning and region-aware prompting. Similarly to the recent work on LLM-based single-objective optimization [Schwanke *et al.*, 2025], our method decomposes the search space into smaller sub-regions, balances exploration-exploitation through a composite scoring function, and prompts the LLM to generate candidates in the selected promising sub-regions. However, differently from [Schwanke *et al.*, 2025], we define a novel regional Hypervolume contribution score which is used both as exploitation factor and for the uncertainty component computation. We refer to Figure 1 for an illustration of the pipeline.

To summarize, our key contributions are:

- We introduce MOHOLLM, a hierarchical LLM-based MOO method that enforces structured exploration via adaptive input space partitioning and a composite utility function combining regional Hypervolume contribution, geometric, and uncertainty-driven criteria. (Section 3)
- Under standard regularity and LLM behavior assumptions, we prove that MOHOLLM ensures asymptotic coverage of the true Pareto set. (Section 4)
- Experiments on 15 synthetic and real-world benchmarks show that MOHOLLM is superior to global LLM-based optimizers and is on par with state-of-the-art MOBO and MOEAs. (Section 5)

Together, these contributions enable a more reliable and principled integration of LLMs into MOO frameworks. We release our code in <https://github.com/arberzela/mohollm.git>.

## 2 Background

### 2.1 Preliminaries

Our goal is to solve the problem of global multi-objective optimization for black-box functions where the underlying gradients are typically unavailable and function evaluations are computationally expensive. Let  $\mathbf{F} : \mathcal{X} \rightarrow \mathbb{R}^M$  be the vector-valued objective function defined over a compact hyperrectangular domain  $\mathcal{X} \subset \mathbb{R}^d$ :

$$\min_{x \in \mathcal{X}} \mathbf{F}(x) = (f_1(x), f_2(x), \dots, f_M(x))^\top. \quad (1)$$

We assume that the objectives are conflicting, meaning no single solution simultaneously optimizes all functions. Therefore, we are interested in a set of non-dominated solutions: the Pareto set  $\mathcal{X}^*$ .

**Definition 2.1.** (*Pareto Dominance*) Given two solutions  $x, x' \in \mathcal{X}$ , we say that  $x$  Pareto dominates  $x'$  (denoted  $x \prec x'$ ) if:

$$\forall i \in \{1, \dots, M\} : f_i(x) \leq f_i(x') \text{ and } \exists j : f_j(x) < f_j(x').$$

**Definition 2.2.** (*Pareto Set*) The Pareto set (also called Pareto optimal set) is the set of all non-dominated solutions in the search space:  $\mathcal{X}^* = \{x \in \mathcal{X} \mid \nexists x' \in \mathcal{X} \text{ such that } x' \prec x\}$

The Pareto front is the image of the Pareto set in objective space:  $\mathcal{F}^* = \{\mathbf{F}(x) \mid x \in \mathcal{X}^*\}$ . Our goal is to generate a sequence of observations  $\mathcal{D}_t$  such that the Pareto set approximation is close to the true Pareto set  $\mathcal{X}^*$ , ensuring dense coverage of the optimal trade-off surface. To quantify solution quality, the Hypervolume (HV) indicator is typically used.

**Definition 2.3 (Hypervolume Indicator).** Let  $\mathcal{Y} \subset \mathbb{R}^M$  be a set of objective vectors and  $\mathbf{r} \in \mathbb{R}^M$  be a reference point dominated by all  $\mathbf{y} \in \mathcal{Y}$ . The Hypervolume indicator  $HV(\mathcal{Y})$  is defined as the Lebesgue measure  $\lambda_{HV}$  of the union of hypercubes formed by each point  $\mathbf{y}$  and the reference point  $\mathbf{r}$ :

$$HV(\mathcal{Y}) = \lambda_{HV} \left( \bigcup_{\mathbf{y} \in \mathcal{Y}} \{\mathbf{z} \in \mathbb{R}^M \mid \mathbf{y} \preceq \mathbf{z} \preceq \mathbf{r}\} \right).$$

### 2.2 Related Work

**Evolutionary Algorithms (EAs).** EAs are a dominant class of population-based heuristics for multi-objective optimization, typically categorized by their selection mechanism. Dominance-based methods [Deb *et al.*, 2002; Deb and Jain, 2014], rely on non-dominated sorting to guide the population toward the Pareto front. MOEA/D [Zhang and Li, 2007] decomposes the problem into multiple single objective subproblems. The aforementioned methods struggle with more than two objectives. To mitigate this, indicator-based methods (e.g., SMS-EMOA [Beume *et al.*, 2007]) directly optimize a quality metric such as Hypervolume, offering robust performance at the cost of higher computational complexity.

**Bayesian Optimization (BO).** BO is a sample-efficient framework for optimizing expensive black-box functions by iteratively updating a probabilistic surrogate and maximizing an acquisition function [Shahriari *et al.*, 2016]. In the multi-objective setting (MOBO), methods typically aim to approximate the Pareto front by maximizing indicators such as Hypervolume. While early approaches relied on scalarization [Knowles, 2006], Expected Hypervolume Improvement (EHVI) [Emmerich *et al.*, 2011] has become the de-facto choice by directly targeting hypervolume maximization. Modern implementations like qEHVI [Daulton *et al.*, 2020; Daulton *et al.*, 2021] further enhance efficiency through parallelizable Monte Carlo integration.

**LLM-based Global Optimization.** Recent research leverages LLMs to guide global optimization by framing the search process as an iterative language generation task [Liu *et al.*, 2024; Yang *et al.*, 2024; Song *et al.*, 2024]. In particular, LLAMBO [Liu *et al.*, 2024] show that LLMs can act as effective candidate generator and surrogate model for sample-efficient single-objective optimization. However, purely LLM-based approaches often struggle with numerical reasoning in continuous domains, a limitation that [Schwanke *et al.*, 2025] tries to address through space partitioning.

**Search Space Partitioning.** Search space partitioning has been shown to be beneficial especially for high-dimensional multi-objective optimization problems. Methods such as MORBO [Daulton *et al.*, 2022] use trust regions, while LaMOO [Zhao *et al.*, 2022] uses adaptive tree-based partitioning based on sample quality. All such instances can be formulated using the Multi-Armed Bandit (MAB) framework, which provides a foundation for region selection, traditionally using axis-aligned partitions [Munos, 2011; Bubeck *et al.*, 2011]. Our work extends these principles to LLM-based optimization, treating each partition as an arm in the MAB problem [Valko *et al.*, 2013].

### 3 The MOHOLLM Algorithm

We now introduce MOHOLLM, a method that solves black-box multi-objective optimization problems with LLMs and search space partitioning. By decomposing the continuous search space into discrete regions, we can apply discrete decision-making strategies to balance exploration and exploitation. The continuous optimization problem can hence be seen as a hierarchical MAB problem [Valko *et al.*, 2013; Grill *et al.*, 2015]. Similarly to [Schwanke *et al.*, 2025], our algorithm (see Algorithm 1 for the pseudocode) consists of five iterative steps:

**1. Adaptive Space Partitioning.** To partition the continuous domain  $\mathcal{X}$  into regions, we employ an adaptive discretization strategy based on KD-trees [Munos, 2011; Valko *et al.*, 2013]. One reason we chose axis-aligned partitioning is because of the easier interpretation of the hyperrectangular region boundaries from the LLM in step 4. At each iteration  $t$ , we construct the tree  $\mathcal{T}_t$  recursively from the observation history  $\mathcal{D}_t = \{(x_i, \mathbf{F}(x_i))\}_{i=1}^t$ , where partitions are defined by splitting along the dimension of maximal variance at the median value. This median-based approach ensures a balanced tree structure, avoiding degenerate empty leaf nodes and positioning less observations on region boundaries. To prevent the partitions from becoming too fine-grained, especially in early iterations, we control the granularity of the tree via a dynamic splitting criterion: a leaf node is refined only if its sample count exceeds a time-dependent threshold  $m_t = m_0 + \lfloor \lambda \log(1+t) \rfloor$ . This schedule serves as a structural regularizer, constraining the tree depth in early iterations to force broad, global exploration, while still allowing the partition diameter to vanish asymptotically.

**2. Region Scoring.** Let  $\mathcal{L}_t = \{R_1, \dots, R_{K_t}\}$  denote the resulting set of  $K_t$  disjoint leaf nodes of the KD-tree at iteration  $t^1$ . To decide on which region to sample next with the LLM, we need to score each region with an utility function, that balances exploration and exploitation, so we do not spend unnecessary resources in uninteresting or suboptimal regions. To this end, we define a scalar utility function  $A_j(t)$  that ranks each partition  $R_j \in \mathcal{L}_t$  based on its (i) contribution to the current Pareto front HV, (ii) geometric properties, and (iii) statistical properties.

**i. Pareto Exploitation ( $\psi_{\text{HV}}$ ):** We measure local utility via the *Regional Hypervolume Contribution*<sup>2</sup>, which quantifies the total contribution that the points of each region  $I_j \subset R_j$  have on the current Pareto front  $\mathcal{F}_t^*$ :

$$\psi_{\text{HV}}(R_j) = \text{HV}(\mathcal{F}_t^*) - \text{HV}(\mathcal{F}_t^* \setminus \{\mathbf{F}(x) \mid x \in I_j\}). \quad (2)$$

This metric aligns the search explicitly with the multiple optimization objectives, prioritizing regions that currently sustain the non-dominated set.  $\psi_{\text{HV}}(R_j) = 0$  and  $\psi_{\text{HV}}(R_j) = 1$  mean that no and all points from region  $R_j$  are in the current Pareto set, respectively.

<sup>1</sup>We write  $R_j$  instead of  $R_{t,j}$  for brevity.

<sup>2</sup>To ensure scale invariance, all objective vectors  $\mathbf{y} \in \mathcal{R}^M$  are min–max normalized to  $[0, 1]$  before HV computation:  $\tilde{\mathbf{y}} = (\mathbf{y} - \mathbf{y}_{\min}) / (\mathbf{y}_{\max} - \mathbf{y}_{\min})$ , with bounds from the current history.

---

#### Algorithm 1 MOHOLLM Algorithm Pseudocode

---

```

Require: Initial data  $\mathcal{D}_{t_0}$ , budget  $T$ , batch size  $b$ , regions  $k$ , candidates  $N$ , initial leaf size  $m_0$ .
1: Initialize  $t \leftarrow t_0$ .
2: while  $t < T$  do
3:   // Step 1: Partitioning
4:   Construct KD-tree  $\mathcal{T}_t$  on  $\mathcal{D}_t$ 
5:   Adjust leaf maximum size  $m_t = m_0 + \lfloor \lambda \log(1+t) \rfloor$ 
6:   // Step 2: Scoring
7:   for each leaf  $R_j$  do
8:     Compute Exploitation:  $\psi_{\text{HV}}(R_j)$  (Eq. 2)
9:     Compute Exploration:
10:       $\psi_{\text{Vol}}(R_j)$  (Eq. 3) &  $\psi_{\text{UCBV}}(R_j)$  (Eq. 4)
11:   Compute composite score  $A_j(t)$  (Eq. 5)
12:   end for
13:   // Step 3: Selection
14:   Compute probabilities of regions  $\pi(t) \propto \exp(\mathbf{A}(t))$ 
15:    $\mathcal{L}_t^{\text{sampled}} \leftarrow$  sample  $k$  regions from  $\text{Cat}(\pi(t))$ 
16:   // Step 4: Sampling
17:   for each  $R \in \mathcal{L}_t^{\text{sampled}}$  do
18:     Generate  $N$  candidates  $\hat{x} \sim p_{\text{LLM}}(x \mid \mathcal{C}(R_j, \mathcal{D}_t))$ 
19:   end for
20:   // Step 5: Evaluation
21:   For all candidates predict  $\hat{\mathbf{y}} \sim p_{\text{LLM}}(\mathbf{y} \mid \mathcal{C}(\mathcal{D}_t, \hat{x}))$ 
22:   Select batch  $B^*$  of size  $b$  maximizing predicted HV
23:   Evaluate true objectives:  $\mathbf{Y}^* \leftarrow \mathbf{F}(B^*)$ 
24:   Update  $\mathcal{D}_t \leftarrow \mathcal{D}_t \cup (B^*, \mathbf{Y}^*)$ 
25:    $t \leftarrow t + b$ 
26: end while
27: return  $\mathcal{F}_{\text{final}}$  (Pareto Front of  $\mathcal{D}_T$ )

```

---

**ii. Geometric Exploration ( $\psi_{\text{Vol}}$ ):** Our first exploration term involves a "void-filling" incentive based on the geometric mean of the side lengths of each leaf hyperrectangular region:

$$\psi_{\text{Vol}}(R_j) = \text{vol}(R_j)^{1/d}, \quad (3)$$

where  $d$  is the input dimensionality.  $\psi_{\text{Vol}}$  ensures that large, under-sampled subspaces retain non-negligible selection probability purely due to their size, thereby preventing the premature exclusion of unvisited regions.

**iii. Statistical Exploration ( $\psi_{\text{UCBV}}$ ):** To assign high importance to regions which have high objective variance, we employ a variance-based Upper Confidence Bound [Audibert and Bubeck, 2009] as a second exploration term:

$$\psi_{\text{UCBV}}(R_j) = \sqrt{\frac{2\varsigma_j^2 \max(0, \ln(\frac{t}{K_t \cdot |I_j|}))}{|I_j|}}, \quad (4)$$

where  $K_t$  is the number of active leaves,  $|I_j|$  is the number of points in region  $R_j$  and  $\varsigma_j^2 = \text{Var}(\{\text{HV}(\mathcal{F}_t^*) - \text{HV}(\mathcal{F}_t^* \setminus \{\mathbf{F}(x)\}_{x \in I_j})\})$  is the variance contribution of each point to the current Pareto front HV.

The final score aggregates these components via a non-linear scalarization:

$$A_j(t) = \sigma(\psi_{\text{HV}}(R_j)) + \alpha_t [\beta_1 \sigma(\psi_{\text{Vol}}(R_j)) + \beta_2 \sigma(\psi_{\text{UCBV}}(R_j))], \quad (5)$$

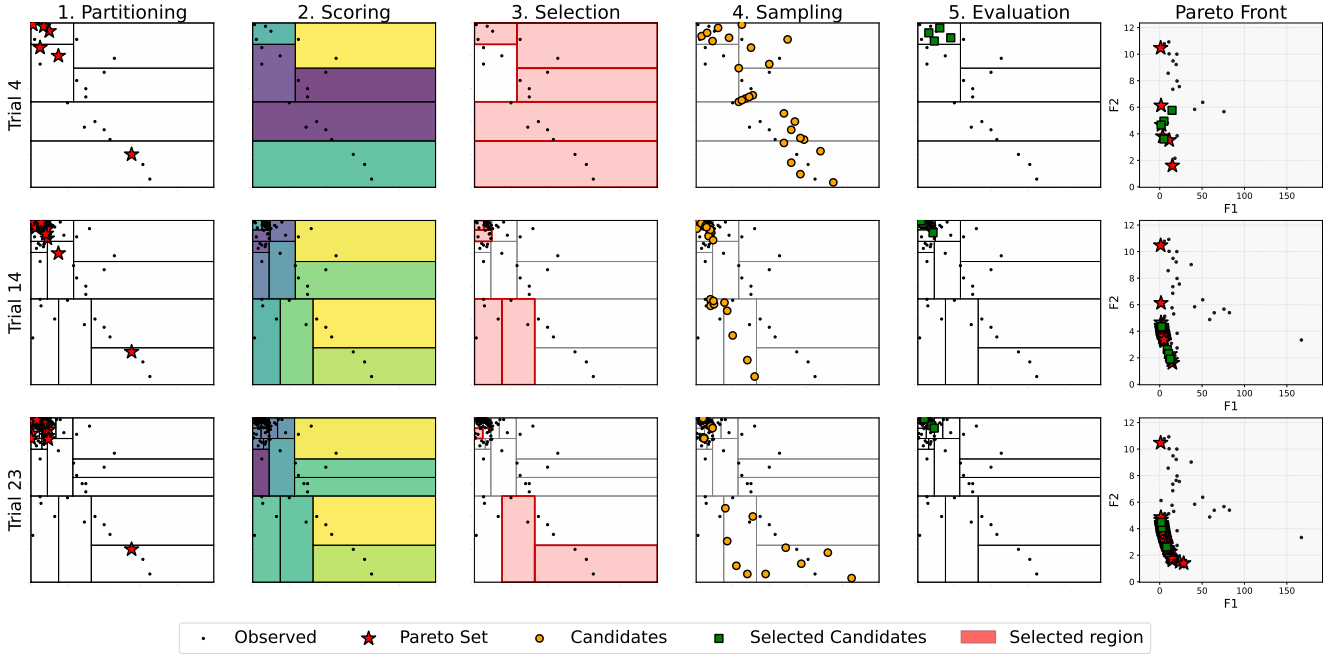


Figure 2: Search process of MOHOLLM on the 2D Branin–Curnin function at different optimization stages. The last column illustrates the function values, while other columns the five algorithmic steps: partitioning, region scoring, probabilistic selection, LLM-based sampling, and evaluation. Rows correspond to early, intermediate, and late trials. MOHOLLM transitions from coarse, globally exploratory partitions to fine-grained, localized refinement around the Pareto front, allocating samples to both sparse regions and dense Pareto-optimal areas.

where  $\beta_1 + \beta_2 = 1$ . The sigmoid function  $\sigma(\cdot)$  normalizes the different ranges from each component into a common  $[0, 1]$  interval.  $\alpha_t$  is a temperature parameter that decays following a cosine annealing schedule as  $t$  increases, therefore suppressing the exploration terms  $(\psi_{\text{Vol}}, \psi_{\text{UCBV}})$  to enforce a more exploitative search in later iterations.

**3. Stochastic Region Selection.** We employ a stochastic selection policy instead of a greedy one in favor of regions with maximal score. The selection probability  $\pi_j(t)$  for region  $R_j$  at iteration  $t$  is defined via the Softmax function:

$$\pi_j(t) = \frac{\exp(A_j(t))}{\sum_{k=1}^{K_t} \exp(A_k(t))}. \quad (6)$$

We denote with  $\mathbf{A} = (A_1, \dots, A_{K_t})$  the vector of scores,  $\boldsymbol{\pi} = (\pi_1, \dots, \pi_{K_t})$  the vector of probability masses and with  $\text{Cat}(\boldsymbol{\pi})$  the Categorical distribution over  $\mathcal{L}_t$ , where we sample  $k \leq K_t$  regions without repetition. This stochastic formulation guarantees that every active region retains a strictly positive selection probability  $\pi_j > 0$ , thereby infinite visit count in the limit (consistent with Assumption 4.3 in Section 4), a necessary condition for almost-sure convergence to the Pareto set, which we prove in Section 4.

**4. LLM-based Generative Sampling.** After sampling a subset  $\mathcal{L}_t^{\text{sampled}} \subset \mathcal{L}_t$  of  $k$  regions from  $\text{Cat}(\boldsymbol{\pi})$ , we deploy a LLM as a local conditional sampler to generate  $N$  new candidate points inside these sampled regions:

$$\hat{x} \sim p_{\text{LLM}}(x \mid \mathcal{C}(R_j, \mathcal{D}_t)), \quad (7)$$

where  $\mathcal{C}$  denotes the prompt construction function. A prompt instance provided to the LLM has the following simplified

instructions (see Appendix F for the full prompt templates): “Given the history of evaluations  $\mathcal{D}_t$ , generate  $N$  new candidate points within the region  $R_j$ .”. The use of LLMs in this setting is motivated from two main reasons. First, the LLM can be seen as flexible non-parametric generators, with a very rich prior (result of pre-training), that does not require assumptions on functions as, for instance, GPs do [Rasmussen and Williams, 2006]. Second, in-context learning enables quick adaptation to diverse tasks without the need of retraining [Brown *et al.*, 2020; Krishnamurthy *et al.*, 2024].

**5. LLM-based Surrogate Modeling and Evaluation.** At each iteration of MOHOLLM, we evaluate the true functions on a batch  $b$  of new points. However, in step 4 we generated  $k \cdot N$  candidates ( $N$  candidates in  $k$  regions) using the LLM. Typically,  $k \cdot N > b$ , so we need a strategy to select the subset of  $b$  points. To this end, similarly as in step 4, we again utilize the LLM’s capabilities to act as a performance predictor (surrogate model), generating predicted objective values  $\hat{y} \sim p_{\text{LLM}}(y \mid \mathcal{C}(\mathcal{D}_t, \hat{x}))$  for the entire pool of generated candidates. From this synthetic pool, we then select a batch  $B^*$  of size  $b$  that maximizes the predicted HV indicator. Only this optimized batch is evaluated on the expensive true functions. Finally, we update the history of evaluations  $\mathcal{D}_t$  with the new points and repeat the above steps until we reach the total evaluation budget  $T$ .

**Search Process Visualization.** In Figure 2 we illustrate MOHOLLM’s search on the 2D BraninCurnin (see Figure 7 and 8 in Appendix E for Chankong-Haines and Poloni, respectively). Early iterations (Trial 4) show coarse partitions

encouraging global exploration, while later iterations (Trial 23) show fine-grained partitions focused on promising regions. The region scoring consistently balances exploration and exploitation by allocating resources to both sparse regions and dense Pareto-front regions simultaneously.

## 4 Theoretical Analysis

Let  $\mathcal{X} \subset \mathbb{R}^d$  be a compact hyperrectangular domain and let  $\mathcal{X}^* \subset \mathcal{X}$  denote the Pareto set induced by the vector-valued objective  $\mathbf{F} = (f_1, \dots, f_M)$ . Let  $\mathcal{S}_t = \{x_1, \dots, x_t\}$  be the set of points sampled by MOHOLLM up to iteration  $t$ . To quantify convergence, we adopt the (directed) Hausdorff distance:  $d_H(\mathcal{X}^*, \mathcal{S}_t) = \sup_{x^* \in \mathcal{X}^*} \inf_{x \in \mathcal{S}_t} \|x - x^*\|_2$ , a set distance metric commonly used in multi-objective optimization. Our goal is to show that, under mild and standard regularity assumptions, which we adopt from optimistic and hierarchical optimization theory [Munos, 2011; Bubeck *et al.*, 2011], and assumptions regarding the stochastic selection and LLM sampling,  $d_H(\mathcal{X}^*, \mathcal{S}_t) \rightarrow 0$  almost surely, implying that every Pareto-optimal point is approximated arbitrarily well by MOHOLLM's sampled points.

**Assumption 4.1** (Lipschitz Continuity). Each objective  $f_i : \mathcal{X} \rightarrow \mathbb{R}$  is Lipschitz continuous. Thus,  $\mathbf{F}$  is continuous and maps compact sets to compact sets.

This standard condition links spatial resolution to approximation error, bounding objective changes under small decision-space perturbations.

**Assumption 4.2** (Hierarchical Partitioning). MOHOLLM maintains a hierarchical partition of  $\mathcal{X}$  using a KD-tree. Let  $R_t(x)$  denote a leaf region containing  $x$  at iteration  $t$ . For any infinite sequence of nested regions,  $R_1 \supset R_2 \supset \dots$ , generated along a branch of the tree, we assume  $\lim_{t \rightarrow \infty} \text{diam}(R_t) = 0$ .

This assumption guarantees that recursive refinement can localize arbitrarily small neighborhoods. It is satisfied by standard axis-aligned splitting rules and is a cornerstone of convergence proofs for hierarchical optimistic optimization [Munos, 2011; Bubeck *et al.*, 2011].

**Assumption 4.3** (Sufficient Exploration). For any leaf region  $R_k$  created at  $t_0$ , the selection probabilities  $\pi_k(t)$  satisfy  $\sum_{t=t_0}^{\infty} \pi_k(t) = \infty$  almost surely.

This is a non-starvation condition ensuring that every region that persists in the tree is sampled infinitely often. In MOHOLLM, region scores are bounded through a sigmoid transformation, and the resulting Softmax normalization yields  $\pi_k(t) = \Omega(1/K_t)$ , where  $K_t$  is the number of leaf nodes. If  $K_t \leq t$ , e.g. in a fixed tree, the series diverges by comparison with the harmonic series.

**Assumption 4.4** (Eventual Refinement). Any leaf region  $R$  selected infinitely often is split infinitely often, producing child regions of strictly smaller diameter.

This assumption prevents stagnation at a fixed spatial resolution, mirroring refinement guarantees used in optimistic tree search [Kleinberg *et al.*, 2008; Bubeck *et al.*, 2011].

**Assumption 4.5** (LLM Sampling). Let  $p_{\text{LLM}}(x \mid \mathcal{C}(R_j, \cdot))$  denote the conditional density of the LLM-generated proposal given region  $R_j$ . For any measurable ball  $B \subset R$ , there exists  $\eta > 0$  such that

$$\int_B P_{\text{LLM}}(x \mid \mathcal{C}(R_j, \cdot)) dx \geq \eta \frac{\text{vol}(B)}{\text{vol}(R_j)}.$$

With this assumption, we ensure that the LLM assigns non-zero probability mass to any subregion  $B$  inside the selected region  $R_j$ , hence avoiding complete mode collapse.

The aforementioned assumptions guarantee that MOHOLLM balances global exploration with local refinement, ensuring asymptotic coverage of the Pareto set without relying on parametric surrogates. Before proving such claim, we first establish an intermediate result regarding the spatial resolution of the partition around optimal points.

**Lemma 4.6** (The Shrinking Lemma). *For any  $x^* \in \mathcal{X}^*$ , the diameter of the leaf node containing  $x^*$  converges to zero almost surely, i.e.  $\lim_{t \rightarrow \infty} \text{diam}(R_t(x^*)) = 0$  a.s.*

*Proof.* We use contradiction for the proof. Assume that the diameter does not converge to zero. Given the hierarchical nature of the partition, this implies that after some finite time  $T_0$ , the leaf  $\bar{R} = R_{T_0}(x^*)$  is never split again. Since  $\bar{R}$  remains a leaf for all  $t > T_0$ , Assumption 4.3 ensures that its cumulative selection probability diverges:  $\sum_{t=T_0}^{\infty} \pi_{\bar{R}}(t) = \infty$ . By the second Borel-Cantelli lemma, this series' divergence implies that  $\bar{R}$  is selected infinitely often. However, Assumption 4.4 requires that any region selected infinitely often must eventually split. This contradicts the assumption that  $\bar{R}$  remains fixed after some time. Consequently, the sequence of regions containing  $x^*$  must undergo infinite refinement, driving the diameter to zero (Assumption 4.2).  $\square$

**Theorem 4.7** (Almost-Sure Pareto Consistency). *Under Assumptions 4.1–4.4, the sample set  $\mathcal{S}_t$  converges to the Pareto set  $\mathcal{X}^*$  in the Hausdorff distance almost surely:*

$$\lim_{t \rightarrow \infty} d_H(\mathcal{X}^*, \mathcal{S}_t) = 0 \quad \text{a.s.}$$

*Proof.* Since  $\mathcal{X}^*$  is compact, it suffices to show that for any  $\varepsilon > 0$  and any target  $x^* \in \mathcal{X}^*$ , the algorithm eventually places a sample inside the open ball  $B(x^*, \varepsilon)$ . Fix  $x^* \in \mathcal{X}^*$  and  $\varepsilon > 0$ . By Lemma 4.6, the diameter of the containing cell  $R_t(x^*)$  converges to 0 almost surely. Thus, there exists a finite time  $T_{\text{loc}}$  such that for all  $t > T_{\text{loc}}$ ,  $R_t(x^*) \subset B(x^*, \varepsilon/2)$ .

For  $t > T_{\text{loc}}$ , any sample generated within  $R_t(x^*)$  necessarily lies within  $B(x^*, \varepsilon)$ . From the proof of Lemma 4.6, we know that the sequence of regions  $\{R_t(x^*)\}_t$  is selected infinitely often. Let  $\{t_k\}$  be the sequence of iterations where such a selection occurs. By Assumption 4.5, conditioned on selecting  $R_{t_k}(x^*)$ , the LLM generates a valid point  $\hat{x}_{\text{new}} \in R_{t_k}(x^*)$  with probability at least  $\eta > 0$ . The probability that no sample ever lands in  $B(x^*, \varepsilon)$  is bounded by  $\lim_{K \rightarrow \infty} (1 - \eta)^K = 0$ . Thus,  $B(x^*, \varepsilon) \cap \mathcal{S}_t \neq \emptyset$  almost surely as  $t \rightarrow \infty$ .

Finally, by compactness,  $\mathcal{X}^*$  admits a finite cover of  $\varepsilon/2$ -balls centered at  $\{z_1, \dots, z_N\}$ . Applying the argument above to each  $z_i$  simultaneously, there exists a time  $T$  such

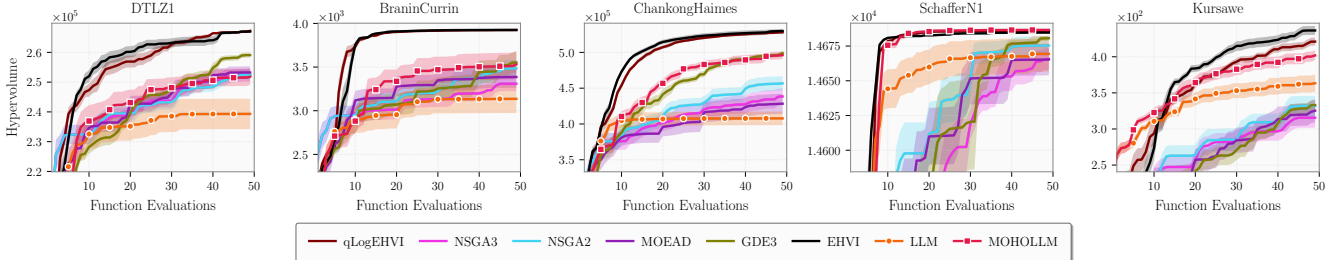


Figure 3: Hypervolume (HV) over function evaluations on synthetic benchmarks (DTLZ1, Branin-Currin, Chankong–Haimes, SchafferN1 and Kursawe). MOHOLLM and the LLM baseline curves are marked to highlight them further.

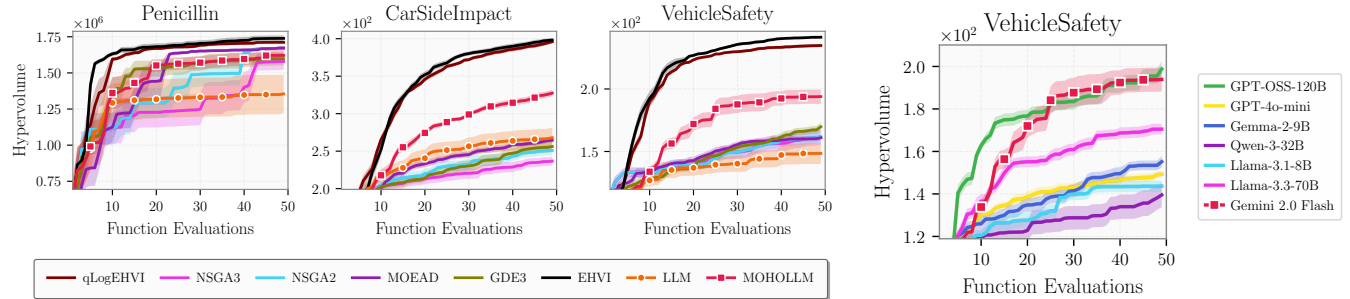


Figure 4: Hypervolume (HV) of MOHOLLM and baselines over function evaluations on real-world benchmarks (Penicillin, Vehicle Safety, and Car Side Impact).

Figure 5: HV trajectories of MOHOLLM with different LLM surrogates and samplers.

that  $\mathcal{S}_T$  intersects every ball in the cover. This implies  $\sup_{x^* \in \mathcal{X}^*} \inf_{x \in \mathcal{S}_T} \|x - x^*\| < \varepsilon$ . Since  $\varepsilon$  is arbitrary, the Hausdorff distance converges to 0 almost surely.  $\square$

**Corollary 4.8** (Hypervolume Consistency). *The hypervolume of the objective vectors  $\mathbf{F}(\mathcal{S}_t)$  converges to the hypervolume of the true Pareto Front  $\mathbf{F}(\mathcal{X}^*)$  almost surely.*

*Proof.* Theorem 4.7 establishes that  $\lim_{t \rightarrow \infty} d_H(\mathcal{X}^*, \mathcal{S}_t) = 0$ . Since  $\mathbf{F}$  is Lipschitz continuous (Assumption 4.1), this implies that the image  $\mathbf{F}(\mathcal{S}_t)$  converges to the true Pareto front  $\mathbf{F}(\mathcal{X}^*)$  in the objective space. Since the HV is Lipschitz continuous w.r.t.  $d_H$  on compact domains, the convergence of  $\mathbf{F}(\mathcal{S}_t)$  guarantees the convergence of the HV too.  $\square$

## 5 Numerical Experiments

**Benchmarks.** We evaluate MOHOLLM on 15 low- to mid-dimensional multi-objective (up to 4 objectives) problems from the `pymoo` [Blank and Deb, 2020] and `BoTorch` [Balandat *et al.*, 2020] libraries: 12 synthetic (DTLZ1-3, BraninCurrin, ChankongHaimes, GMM, Poloni, SchafferN1-2, TestFunction4, ToyRobust, Kursawe) and 3 real-world (Penicillin fermentation, VehicleSafety, CarSideImpact). See Appendix A for details on each benchmark.

**Baselines.** We compare against 2 standard MOBO methods and 11 MOEAs. Full details on these methods are provided in Appendix B. Additionally, to clearly encapsulate the effect of our algorithmic design choices, we also compare to a global LLM baseline (see Algorithm 2), that uses the exact same prompt templates and evaluation scheme as MOHOLLM, but always has only a global view of the input space.

**Configuration.** Unless stated otherwise, MOHOLLM uses `Gemini-2.0-Flash` with the following default hyperparameters:  $k = 5$  regions,  $N = 5$  candidates per region,  $b = 4$  evaluations per trial,  $m_0 = 5$ ,  $\alpha_{\max} = 1.0$  (decaying to 0.01),  $\beta_1 = \beta_2 = 0.5$ . In Appendix E, we study the robustness of MOHOLLM towards these hyperparameter choices. We utilize the prompts templates as illustrated in Section F. We run each method for 50 function evaluations (including the 5 initial random samples) 10 times with different random seeds and report the mean  $\text{HV} \pm 95\%$  confidence interval (CI).

### 5.1 Results on Synthetic Benchmarks

Results in Figure 3 (see Figure 9 in Appendix E for results on all benchmarks) show that MOHOLLM demonstrates consistent improvement compared to the global LLM baseline throughout the full evaluation budget across most benchmarks. This indicates that MOHOLLM is able to find diverse solution sets across problems with different Pareto front characteristics – from the linear and convex fronts of DTLZ1, Chankong–Haimes and SchafferN1 to the disconnected, highly nonconvex fronts of Branin-Currin and Kursawe. Although MOHOLLM does not surpass the competitive MOBO methods, which are known to work particularly well for small evaluation budgets, its performance places it within the competitive range of established MOEAs.

### 5.2 Results on Real-World Benchmarks

Real-world applications usually involve expensive-to-evaluate objectives, e.g., mechanical simulations or chemical processes. We consider the problems of optimizing VehicleSafety for side-impact collisions based on established crash

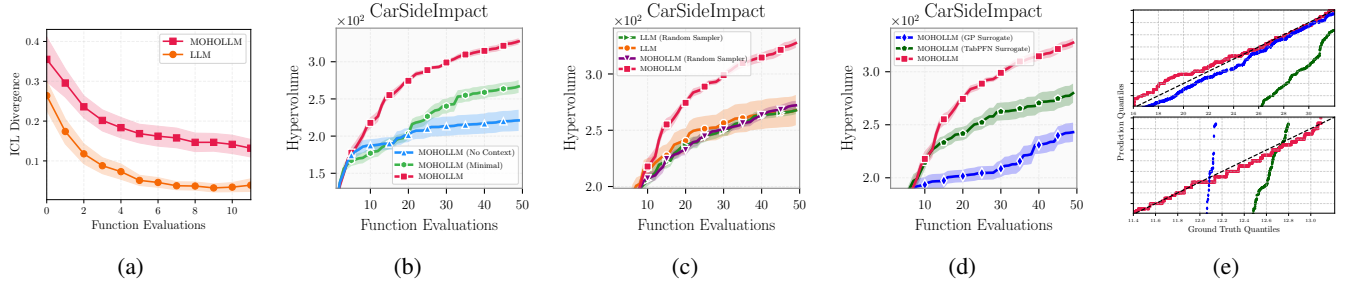


Figure 6: Ablation and analysis results. (a) Aggregate ICL divergence over function evaluations. (b) Prompt ablations. (c) Candidate sampler ablation comparing LLM-based and random sampling strategies. (d) Surrogate model ablation comparing LLM, GP, and TabPFN-v2 surrogates. (e) Q-Q plot on 2 objectives from CarSideImpact, comparing predicted versus true objective value distributions.

simulations (CarSideImpact;  $d = 7, M = 4$ ) and its crash-worthiness design during a frontal impact (VehicleSafety,  $d = 5, M = 3$ ) [Liang and Lai, 2021]. Conflicting objectives involve balancing the weight of a car (low weight brings lower manufacturing cost and less fuel consumption) and its damage to both the car and passengers during collision (lighter materials leads to more damage). We also evaluate MOHOLL on the Penicillin production problem ( $d = 7, M = 3$ ) [Tanabe and Ishibuchi, 2020], where the objective is to maximize penicillin yield while simultaneously minimizing fermentation time and CO<sub>2</sub> emissions by optimizing seven initial reaction conditions.

As shown in Figure 4 (see Figure 10 for results with more MOEAs and Figure 11 for the Pareto front plots), the global LLM baseline likely gets stuck exploiting sub-optimal regions, hence explaining low and stagnating HV on all tasks. On the other hand, although MOBO methods [Daulton *et al.*, 2020; Emmerich *et al.*, 2011] remain superior on real-world tasks due to their sample efficiency, MOHOLL consistently shows stronger performance than all MOEAs while avoiding the premature convergence of the global LLM-based search.

### 5.3 Analysis and Ablations

**Impact of LLM type/size.** Testing different LLMs on VehicleSafety (Figure 5) shows a hierarchy in performance. Top performers (Gemini-2.0-Flash, GPT-OSS-120B, LLaMA-3.3-70B) are larger models optimized for instruction-following and reasoning. Smaller models (LLaMA-3.1-8B, Gemma-2-9B, Qwen3-32B) show significantly worse performance, suggesting that the LLM size and capabilities are relevant for such tasks. In Appendix C we provide operational costs' breakdown for using each model.

**Sample Diversity.** To quantify exploration we compute the average distance of generated proposals from the historical evaluated examples:  $D_{\text{ICL}} = 1/|S| \sum_{s \in S} \min_{i \in I} d(s, i)$ , where  $S$  are new proposals,  $I$  are the examples, and  $d(\cdot, \cdot)$  is Euclidean distance in the normalized unit hypercube. We call this metric in-context learning (ICL) divergence. Figure 6a plots the aggregated ICL divergence across all benchmarks. We can see that MOHOLL generates more diverse (higher ICL div.) candidates at each iteration compared to the global LLM sampler, demonstrating that the search space partitioning enforces more in-region exploration and prevents mode collapse (also in line with Assumption 4.5 from Section 4).

**Prompt Variations.** We evaluate Context (default MOHOLL setting with problem description in prompts), No Context, and Minimal prompts to assess the utility of domain knowledge in optimization (prompt variations shown in Appendix F). Real-world benchmark results in Figure 6b and Figure 12 indicate that providing task context in the prompts typically results in better performance of MOHOLL.

### Impact of LLMs as Surrogate Models and Candidate Samplers.

We also quantify the LLM contribution by isolating its roles in MOHOLL. As a candidate sampler, we see from Figure 6c that MOHOLL significantly outperforms its variant with random uniform sampling, both globally or inside input space partitions, confirming its ability to generate more informative proposals. As a surrogate model, the LLM (Gemini-2.0-Flash) demonstrates reliable predictive performance on the real-world tasks, as shown in Figure 6d and the Q-Q plot in Figure 6e, achieving a high Spearman rank correlation (0.874) and  $R^2$  (0.757). In contrast, Gaussian Processes [Rasmussen and Williams, 2006] and TabPFN-v2 [Hollmann *et al.*, 2025] fail to capture the objective structure, exhibiting near-zero correlations and highly negative  $R^2$  scores in some objectives. We provide additional results on the other real-world benchmarks in Appendix E.

## 6 Conclusion and Discussion

We proposed MOHOLL, a method that improves LLM-based multi-objective optimization through hierarchical space partitioning and a multi-armed bandit-inspired scoring for the resulting regions. Extensive experimental evaluations across 15 benchmarks, demonstrated that MOHOLL showed consistent improvements compared to the global LLM-based baseline, while at the same time being competitive with established multi-objective evolutionary algorithms. We expect that MOHOLL will open a pathway towards faithful integration of LLMs in multi-objective optimization.

Our method has also some limitations. The current reliance on axis-aligned KD-trees makes applicability to non-Euclidean domains not trivial. Furthermore, LLM inference cost increase with the problem dimensionality, making it hard for MOHOLL to run on high evaluation budgets. Finally, while we established Pareto consistency, deriving formal asymptotic Hypervolume regret bounds [Zhao *et al.*, 2022; Golovin and Zhang, 2020] remains an open future problem.

## References

[Agarwal *et al.*, 2025] Dhruv Agarwal, Manoj Ghuhan Arivazhagan, Rajarshi Das, Sandesh Swamy, Sopan Khosla, and Rashmi Gangadharaiah. Searching for optimal solutions with LLMs via bayesian optimization. In *The Thirteenth International Conference on Learning Representations*, 2025.

[Ament *et al.*, 2023] Sebastian Ament, Sam Daulton, David Eriksson, Maximilian Balandat, and Eytan Bakshy. Unexpected improvements to expected improvement for bayesian optimization. In *Advances in Neural Information Processing Systems 37*, 2023.

[Audibert and Bubeck, 2009] Jean-Yves Audibert and Sébastien Bubeck. Minimax policies for adversarial and stochastic bandits. In *Proceedings of the 22th annual conference on learning theory*, pages 217–226, Montreal, Canada, June 2009.

[Balandat *et al.*, 2020] Maximilian Balandat, Brian Karrer, Daniel R. Jiang, Samuel Daulton, Benjamin Letham, Andrew Gordon Wilson, and Eytan Bakshy. BoTorch: A Framework for Efficient Monte-Carlo Bayesian Optimization. In *Advances in Neural Information Processing Systems 33*, 2020.

[Beume *et al.*, 2007] Nicola Beume, Boris Naujoks, and Michael Emmerich. Sms-emoa: Multiobjective selection based on dominated hypervolume. *European Journal of Operational Research*, 181(3):1653–1669, 2007.

[Blank and Deb, 2020] J. Blank and K. Deb. pymoo: Multi-objective optimization in python. *IEEE Access*, 8:89497–89509, 2020.

[Brown *et al.*, 2020] Tom Brown, Benjamin Mann, Nick Ryder, et al. Language models are few-shot learners. *Advances in Neural Information Processing Systems*, 2020.

[Bubeck *et al.*, 2011] Sébastien Bubeck, Rémi Munos, Gilles Stoltz, and Csaba Szepesvári. X-armed bandits. *J. Mach. Learn. Res.*, 12(null):1655–1695, July 2011.

[Chinchuluun and Pardalos, 2007] Altannar Chinchuluun and Panos Pardalos. A survey of recent developments in multiobjective optimization. *Annals of Operations Research*, 154(1):29–50, October 2007.

[Coello Coello, 1999] Carlos A. Coello Coello. A comprehensive survey of evolutionary-based multiobjective optimization techniques. *Knowl. Inf. Syst.*, 1(3):269–308, August 1999.

[Corne *et al.*, 2001] David W Corne, Nick R Jerram, Joshua D Knowles, and Martin J Oates. PESA-II: Region-based selection in evolutionary multiobjective optimization. In *Proceedings of the genetic and evolutionary computation conference*, pages 283–290, 2001.

[Daulton *et al.*, 2020] Samuel Daulton, Maximilian Balandat, and Eytan Bakshy. Differentiable Expected Hypervolume Improvement for Parallel Multi-Objective Bayesian Optimization. In *Advances in Neural Information Processing Systems 33*, 2020.

[Daulton *et al.*, 2021] Samuel Daulton, Maximilian Balandat, and Eytan Bakshy. Parallel bayesian optimization of multiple noisy objectives with expected hypervolume improvement. In *Advances in Neural Information Processing Systems 34*, 2021.

[Daulton *et al.*, 2022] Samuel Daulton, David Eriksson, Maximilian Balandat, and Eytan Bakshy. Multi-objective bayesian optimization over high-dimensional search spaces. In *Proceedings of the Thirty-Eighth Conference on Uncertainty in Artificial Intelligence*, 2022.

[Deb and Jain, 2014] Kalyanmoy Deb and Himanshu Jain. An evolutionary many-objective optimization algorithm using reference-point-based nondominated sorting approach, part i: solving problems with box constraints. *IEEE transactions on evolutionary computation*, 18(4):577–601, 2014.

[Deb and Sundar, 2006] Kalyanmoy Deb and Jinayandanan Sundar. Reference point based multi-objective optimization using evolutionary algorithms. In *Proceedings of the 8th annual conference on Genetic and evolutionary computation*, pages 635–642, 2006.

[Deb *et al.*, 2002] Kalyanmoy Deb, Amrit Pratap, Sameer Agarwal, and TAMT Meyarivan. A fast and elitist multiobjective genetic algorithm: Nsga-ii. *IEEE transactions on evolutionary computation*, 6(2):182–197, 2002.

[Deb, 2001] Kalyanmoy Deb. *Multi-objective optimization using evolutionary algorithms*. John Wiley & Sons, 2001.

[Emmerich *et al.*, 2011] Michael T. M. Emmerich, André H. Deutz, and Jan Willem Klinkenberg. Hypervolume-based expected improvement: Monotonicity properties and exact computation. In *IEEE Congress of Evolutionary Computation (CEC)*, 2011.

[Golovin and Zhang, 2020] Daniel Golovin and Qiuyi (Richard) Zhang. Random hypervolume scalarizations for provable multi-objective black box optimization. In *Proceedings of the 37th International Conference on Machine Learning*, 2020.

[Gopakumar *et al.*, 2018] Abhijith M. Gopakumar, Prasanna V. Balachandran, Dezhen Xue, James E. Gubernatis, and Turab Lookman. Multi-objective optimization for materials discovery via adaptive design. *Scientific Reports*, 8(1):3738, 2018.

[Grill *et al.*, 2015] Jean-Bastien Grill, Michal Valko, Remi Munos, and Remi Munos. Black-box optimization of noisy functions with unknown smoothness. In *Advances in Neural Information Processing Systems 28*, 2015.

[Hollmann *et al.*, 2025] Noah Hollmann, Samuel Müller, Lennart Purucker, Arjun Krishnakumar, Max Körfer, Shi Bin Hoo, Robin Tibor Schirrmeyer, and Frank Hutter. Accurate predictions on small data with a tabular foundation model. *Nature*, 01 2025.

[Jones *et al.*, 1998] Donald R. Jones, Matthias Schonlau, and William J. Welch. Efficient global optimization of expensive black-box functions. *J. Global Optimization*, 13(4):455–492, 1998.

[Kleinberg *et al.*, 2008] Robert Kleinberg, Aleksandrs Slivkins, and Eli Upfal. Multi-armed bandits in metric spaces. In *Proceedings of the Fortieth Annual ACM Symposium on Theory of Computing*, 2008.

[Knowles, 2006] Joshua D Knowles. Parego: a hybrid algorithm with on-line landscape approximation for expensive multiobjective optimization problems. *IEEE Transactions on Evolutionary Computation*, 10(1):50–66, 2006.

[Krishnamurthy *et al.*, 2024] Akshay Krishnamurthy, Keegan Harris, Dylan J. Foster, Cyril Zhang, and Aleksandrs Slivkins. Can large language models explore in-context? In *Advances in Neural Information Processing Systems*, 2024.

[Kukkonen and Lampinen, 2005] Saku Kukkonen and Jouni Lampinen. Gde3: The third evolution step of generalized differential evolution. In *2005 IEEE congress on evolutionary computation*, volume 1, pages 443–450, 2005.

[Li *et al.*, 2018] Ke Li, Renzhi Chen, Guangtao Fu, and Xin Yao. Two-archive evolutionary algorithm for constrained multiobjective optimization. *IEEE Transactions on Evolutionary Computation*, 23(2):303–315, 2018.

[Liang and Lai, 2021] Qiaohao Liang and Lipeng Lai. Scalable bayesian optimization accelerates process optimization of penicillin production. In *NeurIPS 2021 AI for Science Workshop*, 2021.

[Liu *et al.*, 2024] Tennison Liu, Nicolás Astorga, Nabeel Seedat, and Mihaela van der Schaar. Large language models to enhance bayesian optimization. In *The Twelfth International Conference on Learning Representations*, 2024.

[Marler and Arora, 2004] R. Timothy Marler and Jasbir Arora. Survey of multi-objective optimization methods for engineering. *Structural and Multidisciplinary Optimization*, 26:369–395, 2004.

[Munos, 2011] Rémi Munos. Optimistic optimization of a deterministic function without the knowledge of its smoothness. In *Advances in Neural Information Processing Systems*, volume 24, 2011.

[OpenAI, 2023] OpenAI. Gpt-4 technical report. *arXiv preprint arXiv:2303.08774*, 2023.

[Rasmussen and Williams, 2006] Carl Edward Rasmussen and Christopher K. I. Williams. *Gaussian Processes for Machine Learning*. The MIT Press, 2006.

[Schwanke *et al.*, 2025] Andrej Schwanke, Lyubomir Ivanov, David Salinas, Fabio Ferreira, Aaron Klein, Frank Hutter, and Arber Zela. Improving llm-based global optimization with search space partitioning. *arXiv preprint, abs/2505.21372*, 2025.

[Seada and Deb, 2016] Haitham Seada and Kalyanmoy Deb. A unified evolutionary optimization procedure for single, multiple, and many objectives. *IEEE Transactions on Evolutionary Computation*, 20(3):358–369, 2016.

[Sener and Koltun, 2018] Ozan Sener and Vladlen Koltun. Multi-task learning as multi-objective optimization. In *Advances in Neural Information Processing Systems* 32, 2018.

[Shahriari *et al.*, 2016] Bobak Shahriari, Kevin Swersky, Ziyu Wang, Ryan P Adams, and Nando De Freitas. Taking the human out of the loop: A review of Bayesian optimization. *Proceedings of the IEEE*, 104(1):148–175, 2016.

[Shields *et al.*, 2021] Benjamin J. Shields, Jason Stevens, Jun Li, Marvin Parasram, Farhan Damani, Jesus I. Martinez Alvarado, Jacob M. Janey, Ryan P. Adams, and Abigail G. Doyle. Bayesian reaction optimization as a tool for chemical synthesis. *Nature*, 590(7844):89–96, 2021.

[Song *et al.*, 2024] Xingyou Song, Yingtao Tian, Robert Tjarko Lange, Chansoo Lee, Yujin Tang, and Yutian Chen. Position: leverage foundational models for black-box optimization. In *Proceedings of the 41st International Conference on Machine Learning*, 2024.

[Tanabe and Ishibuchi, 2020] Ryoji Tanabe and Hisao Ishibuchi. An easy-to-use real-world multi-objective optimization problem suite. *Appl. Soft Comput.*, 89(C), April 2020.

[Tesch *et al.*, 2013] Matthew Tesch, Jeff Schneider, and Howie Choset. Expensive multiobjective optimization for robotics. In *2013 IEEE International Conference on Robotics and Automation*, pages 973–980, 2013.

[Touvron and others, 2023] Hugo Touvron et al. Llama 2: Open foundation and fine-tuned chat models, 7 2023.

[Valko *et al.*, 2013] Michal Valko, Alexandra Carpentier, and Rémi Munos. Stochastic simultaneous optimistic optimization. In *Proceedings of the 30th International Conference on Machine Learning*, 2013.

[Yang *et al.*, 2024] Chengrun Yang, Xuezhi Wang, Yifeng Lu, Hanxiao Liu, Quoc V Le, Denny Zhou, and Xinyun Chen. Large language models as optimizers. In *International Conference on Learning Representations*, 2024.

[Zhang and Li, 2007] Qingfu Zhang and Hui Li. Moea/d: A multiobjective evolutionary algorithm based on decomposition. *IEEE Transactions on evolutionary computation*, 11(6):712–731, 2007.

[Zhang *et al.*, 2023] Michael Zhang, Nishkrit Desai, Juhan Bae, Jonathan Lorraine, and Jimmy Ba. Using large language models for hyperparameter optimization. In *NeurIPS 2023 Foundation Models for Decision Making Workshop*, 2023.

[Zhao *et al.*, 2022] Yiyang Zhao, Linnan Wang, Kevin Yang, Tianjun Zhang, Tian Guo, and Yuandong Tian. Multi-objective optimization by learning space partition. In *International Conference on Learning Representations*, 2022.

[Zitzler and Künzli, 2004] Eckart Zitzler and Simon Künzli. Indicator-based selection in multiobjective search. In *International conference on parallel problem solving from nature*, pages 832–842, 2004.

[Zitzler *et al.*, 2001] Eckart Zitzler, Marco Laumanns, and Lothar Thiele. Spea2: Improving the strength pareto evolutionary algorithm. *TIK-report*, 103, 2001.

## Acknowledgments

Frank Hutter, Arber Zela and David Salinas acknowledge the financial support of the Hector Foundation.

## A Details on Multi-objective Tasks

We evaluate MOHOLLM on a diverse suite of 15 benchmark problems designed to cover a wide range of structural properties encountered in multi-objective optimization.

### A.1 Synthetic Tasks

We utilize the implementation from `pymoo`<sup>3</sup> for the synthetic tasks.

**DTLZ1-3** ( $d = 6, M = 2$ ). The DTLZ test suite defines scalable  $M$ -objective problems over decision variables  $\mathbf{x} = (x_1, \dots, x_d) \in [0, 1]^d$ . For all DTLZ problems, let  $k = d - M + 1$  and

$$g(\mathbf{x}_M) = \sum_{i=M}^d [(x_i - 0.5)^2 - \cos(20\pi(x_i - 0.5))].$$

*DTLZ1* is defined as

$$f_m(\mathbf{x}) = \frac{1}{2}(1+g) \prod_{i=1}^{M-m} x_i \times \begin{cases} 1 - x_{M-m+1}, & m > 1, \\ 1, & m = 1, \end{cases}$$

yielding a linear Pareto front with many local optima induced by  $g$ . *DTLZ2* replaces  $g$  with  $g(\mathbf{x}_M) = \sum_{i=M}^d (x_i - 0.5)^2$  and defines

$$f_m(\mathbf{x}) = (1+g) \prod_{i=1}^{M-m} \cos\left(\frac{\pi}{2}x_i\right) \times \begin{cases} \sin\left(\frac{\pi}{2}x_{M-m+1}\right), & m > 1, \\ 1, & m = 1, \end{cases}$$

resulting in a smooth spherical Pareto front. *DTLZ3* uses the same objectives as DTLZ2 but the multimodal  $g$  of DTLZ1, introducing many deceptive local fronts.

**Branin-Currin** ( $d = 2, M = 2$ ). This bi-objective problem is defined over  $\mathbf{x} = (x_1, x_2) \in [0, 1]^2$ . The first objective is a scaled Branin function:

$$f_1(\mathbf{x}) = \left( x_2 - \frac{5.1}{4\pi^2}x_1^2 + \frac{5}{\pi}x_1 - 6 \right)^2 + 10 \left( 1 - \frac{1}{8\pi} \right) \cos(x_1) + 10,$$

and the second is the Currin function:

$$f_2(\mathbf{x}) = \left( 1 - \exp\left(-\frac{1}{2x_2}\right) \right) \frac{2300x_1^3 + 1900x_1^2 + 2092x_1 + 60}{100x_1^3 + 500x_1^2 + 4x_1 + 20}$$

The conflicting landscapes yield a highly nonconvex Pareto front.

**Chankong-Haines** ( $d = 2, M = 2$ ). A 2-dimensional, 2-objective optimization benchmark defined on the domain  $[-20, 20]^2$ . We use the unconstrained version of this problem, dropping the original constraints, therefore resulting in a convex Pareto front. The objective functions are given by:

$$f_1(x, y) = 2 + (x - 2)^2 + (y - 1)^2$$

$$f_2(x, y) = 9x - (y - 1)^2$$

<sup>3</sup>[https://pymoo.org/problems/test\\_problems.html](https://pymoo.org/problems/test_problems.html)

**GMM** ( $d = 2, M = 2$ ). Defined on the input unit square  $[0, 1]^2$ , it features two objectives, each independently defined by a Gaussian Mixture Model (GMM). The problem is designed for minimization and incorporates multiplicative input noise  $\xi \sim \mathcal{N}(\mu = [1, 1], \Sigma = 0.07I_2)$ , applied before each function evaluation.

**Poloni** ( $d = 2, M = 2$ ). Defined on the domain  $[-\pi, \pi]^2$ , it features a non-convex, disconnected Pareto front. The objective functions are given by:

$$f_1(x, y) = 1 + (A_1 - B_1(x, y))^2 + (A_2 - B_2(x, y))^2$$

$$f_2(x, y) = (x + 3)^2 + (y + 1)^2$$

where the constants  $A_1, A_2$  and terms  $B_1, B_2$  are defined as:

$$A_1 = 0.5 \sin(1) - 2 \cos(1) + \sin(2) - 1.5 \cos(2)$$

$$A_2 = 1.5 \sin(1) - \cos(1) + 2 \sin(2) - 0.5 \cos(2)$$

$$B_1(x, y) = 0.5 \sin(x) - 2 \cos(x) + \sin(y) - 1.5 \cos(y)$$

$$B_2(x, y) = 1.5 \sin(x) - \cos(x) + 2 \sin(y) - 0.5 \cos(y)$$

**SchafferN1** ( $d = 1, M = 2$ ). A classic, 1-dimensional, 2-objective optimization benchmark defined on the domain  $[-10, 10]$  (parameter  $A = 10$ ). It is known for its simple structure but challenging convergence properties. The objectives are:

$$f_1(x) = x^2$$

$$f_2(x) = (x - 2)^2$$

**SchafferN2** ( $d = 1, M = 2$ ). Defined on the domain  $[-5, 10]$ , SchafferN2 features a piecewise linear first objective, adding complexity to the optimization landscape. The objectives are:

$$f_1(x) = \begin{cases} -x & \text{if } x \leq 1 \\ x - 2 & \text{if } 1 < x \leq 3 \\ 4 - x & \text{if } 3 < x \leq 4 \\ x - 4 & \text{if } x > 4 \end{cases}$$

$$f_2(x) = (x - 5)^2$$

**TestFunction4** ( $d = 2, M = 2$ ). Defined on the domain  $[-7, 4]^2$ . While the original problem includes linear constraints, we utilize the unconstrained version in this work. The objective functions are:

$$f_1(x, y) = x^2 - y$$

$$f_2(x, y) = -0.5x - y - 1$$

**ToyRobust** ( $d = 1, M = 2$ ). A benchmark defined on the domain  $[0.0, 0.7]$ , designed such that the Pareto front is sensitive to input noise and is formulated for minimization. The first objective function  $f_1(x)$  is defined as:

$$f_1(x) = -30(p_1(x) \cdot \sigma(x) + p_2(x) \cdot (1 - \sigma(x)) + s(x) + 1)$$

$$\text{where } p_1(x) = 2.4 - 10x - 0.1x^2$$

$$p_2(x) = 2x - 0.1x^2$$

$$s(x) = (x - 0.5)^2 + 0.1 \sin(30x)$$

$$\sigma(x) = \text{sigmoid}((0.2 - x)/0.005)$$

The second objective function  $f_2(x)$  uses a modified 2-dimensional Levy function, applied to a transformed input  $x' = 0.95x + 0.03$  with the second dimension fixed at 0:

$$f_2(x) = \text{Levy}(x', 0) - 0.75(x')^2$$

The  $n$ -dimensional Levy function  $f_{\text{Levy}}(z_1, \dots, z_d)$  is generally defined as:

$$\begin{aligned} f_{\text{Levy}}(z) &= \sin^2(\pi w_1) \\ &+ \sum_{i=1}^{n-1} (w_i - 1)^2 (1 + 10 \sin^2(\pi w_i + 1)) \\ &+ (w_n - 1)^2 (1 + \sin^2(2\pi w_n)) \end{aligned}$$

$$\text{where } w_i = 1 + \frac{z_i - 1}{4} \quad \text{for } i = 1, \dots, d$$

Here,  $n = 2$ ,  $z_1 = x'$ , and  $z_2 = 0$ .

**Kursawe** ( $d = 3, M = 2$ ). A 3-dimensional, 2-objective optimization problem defined on the domain  $[-5, 5]^3$ . It is known for its disconnected Pareto front, making it deceptive and challenging for optimizers regarding solution diversity. The 2 objectives are:

$$\begin{aligned} f_1(x_1, x_2, x_3) &= \sum_{i=1}^2 -10 \exp \left( -0.2 \sqrt{x_i^2 + x_{i+1}^2} \right) \\ f_2(x_1, x_2, x_3) &= \sum_{i=1}^3 (|x_i|^{0.8} + 5 \sin(x_i^3)) \end{aligned}$$

## A.2 Real-world Benchmarks

We utilize the benchmark implementations provided by the `BoTorch` library<sup>4</sup>. These problems represent challenging black-box optimization scenarios characterized by high-dimensional continuous search spaces and conflicting objectives.

**Penicillin Fermentation** ( $d = 7, M = 3$ ) [Liang and Lai, 2021]. This benchmark simulates a fed-batch penicillin production process governed by a system of nonlinear ordinary differential equations (ODEs). The decision vector  $\mathbf{x} \in \mathbb{R}^7$  controls the initial culture volume ( $V$ ), biomass concentration ( $X$ ), temperature ( $T$ ), glucose concentration ( $S$ ), substrate feed rate ( $F$ ), substrate feed concentration ( $s_f$ ), and pH ( $H^+$ ). The simulation evolves over discrete time steps  $t$ , updating state variables according to the following dynamics (simplified for brevity):

$$\begin{aligned} \frac{dV}{dt} &= F - V\lambda(e^{5\frac{T-T_o}{T_v-T_o}} - 1) \\ \frac{dX}{dt} &= \mu(\mathbf{x})X - \frac{X}{V} \frac{dV}{dt} \\ \frac{dS}{dt} &= -\left(\frac{\mu}{Y_{xs}} + \frac{\mu_p}{Y_{ps}} + m_X\right)X + \frac{Fs_f}{V} - \frac{S}{V} \frac{dV}{dt} \\ \frac{dP}{dt} &= \mu_p X - KP - \frac{P}{V} \frac{dV}{dt} \\ \frac{dCO_2}{dt} &= \alpha_1 \frac{dX}{dt} + \alpha_2 X + \alpha_3 \end{aligned}$$

<sup>4</sup>[https://github.com/meta-pytorch/botorch/blob/main/botorch/test\\_functions/multi\\_objective.py](https://github.com/meta-pytorch/botorch/blob/main/botorch/test_functions/multi_objective.py)

where  $\mu$  and  $\mu_p$  are nonlinear growth rates dependent on  $T, S$ , and  $H$ . The optimization minimizes three objectives based on the final state at time  $T_{final}$ :

$$\begin{aligned} f_1(\mathbf{x}) &= -P(T_{final}) \\ f_2(\mathbf{x}) &= CO_2(T_{final}) \\ f_3(\mathbf{x}) &= T_{final} \end{aligned}$$

representing the negative penicillin yield (maximization), total  $\text{CO}_2$  production, and total fermentation time.

**VehicleSafety** ( $d = 5, M = 3$ ) [Tanabe and Ishibuchi, 2020]. This problem optimizes vehicle crashworthiness during a frontal impact. The input  $\mathbf{x} \in [1, 3]^5$  represents the thickness of five structural components: bumper beam ( $x_1$ ), crash box ( $x_2$ ), longitudinal rails ( $x_3$ ), A-pillar ( $x_4$ ), and dash panel ( $x_5$ ).

The three minimization objectives are defined as:

$$\begin{aligned} f_1(\mathbf{x}) &= 1640.2823 + 2.3573285x_1 + 2.3220035x_2 \\ &+ 4.5688768x_3 + 7.7213633x_4 + 4.4559504x_5 \\ f_2(\mathbf{x}) &= 6.5856 + 1.15x_1 - 1.0427x_2 + 0.9738x_3 \\ &+ 0.8364x_4 - 0.3695x_1x_4 + 0.0861x_1x_5 \\ &+ 0.3628x_2x_4 - 0.1106x_1^2 - 0.3437x_3^2 \\ &+ 0.1764x_4^2 \\ f_3(\mathbf{x}) &= -0.0551 + 0.0181x_1 + 0.1024x_2 + 0.0421x_3 \\ &- 0.0073x_1x_2 + 0.024x_2x_3 - 0.0118x_2x_4 \\ &- 0.0204x_3x_4 - 0.008x_3x_5 - 0.0241x_2^2 \\ &+ 0.0109x_4^2 \end{aligned}$$

corresponding to Mass ( $f_1$ ), Acceleration ( $f_2$ ), and Intrusion ( $f_3$ ).

**CarSideImpact** ( $d = 7, M = 4$ ) [Tanabe and Ishibuchi, 2020]. This benchmark addresses side-impact safety. Inputs  $\mathbf{x} \in \mathbb{R}^7$  define the thickness of components like B-pillars and door beams.

The problem defines four minimization objectives:

$$\begin{aligned} f_1(\mathbf{x}) &= 1.98 + 4.9x_1 + 6.67x_2 + 6.98x_3 + 4.01x_4 \\ &+ 1.78x_5 + 10^{-5}x_6 + 2.73x_7 \\ f_2(\mathbf{x}) &= 4.72 - 0.5x_4 - 0.19x_2x_3 \\ f_3(\mathbf{x}) &= 0.5 \cdot (V_{MBP} + V_{FD}) \\ f_4(\mathbf{x}) &= \sum_{i=1}^{10} \max(0, -g_i(\mathbf{x})) \end{aligned}$$

where  $f_1$  is Weight,  $f_2$  is Pubic Force, and  $f_3$  is the average intrusion velocity derived from  $V_{MBP}$  and  $V_{FD}$ .  $f_4$  aggregates violations of 10 structural constraints  $g_i(\mathbf{x})$ .

## A.3 Hypervolume Reference Points

The Hypervolume is computed using the reference points shown in Table 1 for each benchmark. These reference points are chosen to be dominated by all points on the Pareto front, ensuring meaningful Hypervolume calculations. The reference points on the real-world benchmark (Penicillin, Vehicle-Safety and CarSideImpact) have been taken from the `pymoo`

[Blank and Deb, 2020] library. The reference points of the other benchmarks have been computed by identifying the worst point in the pool of all proposals across all runs and methods with an 1% offset.

Table 1: Hypervolume reference points used for performance evaluation across all benchmarks.

Benchmark	Reference Point
DTLZ1	[510.57419, 528.80469]
DTLZ2	[2.2725, 2.2725]
DTLZ3	[1109.84052, 1109.84052]
BraninCurrin	[311.21029, 13.91174]
ChankongHaimes	[936.27, 180.3557]
GMM	[0.0, 0.0]
Poloni	[62.2463, 52.57454]
SchafferN1	[101.0, 145.44]
SchafferN2	[6.06, 101.0]
TestFunction4	[56.56, 9.595]
ToyRobust	[49.995, 37.36394]
Kursawe	[-4.91062, 24.01174]
Penicillin	[25.935, 57.612, 935.5]
CarSideImpact	[45.4872, 4.5114, 13.3394, 10.3942]
VehicleSafety	[1864.72022, 11.81993945, 0.2903999384]

For the real-world benchmarks, the maximum achievable hypervolume is documented in Table 2. The maximum hypervolume was taken from the BoTorch framework.

Table 2: Maximum achievable hypervolume for real-world benchmarks according to the BoTorch framework.

Benchmark	Maximum Hypervolume
Penicillin	2,183,455.909507436
CarSideImpact	484.72654347642793
VehicleSafety	246.81607081187002

## B Baselines

This section provides a brief description of the baseline algorithms used to compare MOHOLLMM throughout this paper. The baselines are grouped into two categories: Multi-Objective Bayesian Optimization (MOBO) methods, primarily implemented in BoTorch [Balandat *et al.*, 2020] and Multi-Objective Evolutionary Algorithms (MOEAs), implemented in pymoo [Blank and Deb, 2020] and platypus<sup>5</sup>. We ran all library-based methods with their standard default parameters.

**Multi-objective Bayesian Optimization Baselines.** We ran two strong standard MOBO baselines.

**EHVI** [Emmerich *et al.*, 2011] The Expected Hypervolume Improvement is a classic MOBO acquisition function that selects the single point that is expected to provide the largest increase to the hypervolume of the current Pareto front approximation.

<sup>5</sup><https://github.com/Project-Platypus/Platypus>

---

### Algorithm 2 Global LLM Baseline Pseudocode

---

**Require:** Initial  $\mathcal{D}_{t_0}$ , budget  $T$ , batch size  $b$ , candidates  $N$ .

- 1: Initialize  $t \leftarrow t_0$ .
- 2: **while**  $t < T$  **do**
- 3:   **// Step 1: Global Sampling**
- 4:   Generate  $N$  candidates  $\hat{x} \sim p_{LLM}(x \mid \mathcal{C}_{global}(\mathcal{D}_t))$
- 5:   **// Step 2: Evaluation**
- 6:   For all candidates predict  $\hat{y} \sim p_{LLM}(y \mid \mathcal{C}(\mathcal{D}_t, \hat{x}))$
- 7:   Select batch  $B^*$  of size  $b$  maximizing predicted HV
- 8:   Evaluate true objectives:  $\mathbf{Y}^* \leftarrow \mathbf{F}(B^*)$
- 9:   Update  $\mathcal{D}_t \leftarrow \mathcal{D}_t \cup (B^*, \mathbf{Y}^*)$
- 10:    $t \leftarrow t + b$
- 11: **end while**
- 12: **return**  $\mathcal{F}_{final}$  (Pareto Front of  $\mathcal{D}_T$ )

---

**qLogEHVI** [Daulton *et al.*, 2020; Ament *et al.*, 2023] A parallelized version of EHVI designed for improved numerical stability during acquisition function optimization. The  $q$  indicates batch evaluation of  $q$  points. The *Log* refers to internal log-transformations and smooth approximations applied during the calculation, preventing the acquisition values and gradients from vanishing numerically, which may be problematic in the standard qEHVI [Ament *et al.*, 2023; Daulton *et al.*, 2020].

**Multi-objective Evolutionary Algorithm Baselines.** We compare MOHOLLMM against a comprehensive suite of 12 established MOEAs that are a standard choice in multi-objective optimization.

**NSGA-II** [Deb *et al.*, 2002] The Non-dominated Sorting Genetic Algorithm II is one of the most widely used and influential MOEAs. It uses a non-dominated sorting procedure for exploitation and a crowding distance mechanism to promote diversity.

**NSGA-III** [Deb and Jain, 2014] An extension of NSGA-II designed to handle many-objective optimization problems. It replaces the crowding distance with a set of pre-defined reference directions to maintain diversity.

**SPEA2** [Zitzler *et al.*, 2001] The Strength Pareto Evolutionary Algorithm 2 is a classic MOEA that uses a concept of strength, which is the number of solutions an individual dominates, and a density estimation technique to guide the search.

**MOEA/D** [Zhang and Li, 2007] The Multi-Objective Evolutionary Algorithm based on Decomposition is a method that decomposes the multi-objective problem into  $N$  single-objective optimization subproblems, each defined by a different weight vector applied to an aggregation function (like Tchebycheff or weighted sum). The algorithm then optimizes these  $N$  subproblems simultaneously in a collaborative manner by defining a *neighborhood* for each subproblem based on the  $T$  closest weight vectors. During optimization, parents for a subproblem are selected only from its neighborhood, and a new solution can replace the current solutions of its neighboring

subproblems, allowing good solutions to spread locally.

**GDE3** [Kukkonen and Lampinen, 2005] The third version of Generalized Differential Evolution, which adapts the Differential Evolution (DE) algorithm for multi-objective constrained optimization. It improves upon earlier GDE versions by incorporating non-dominated sorting and crowding distance.

**IBEA** [Zitzler and Künzli, 2004] The Indicator-Based Evolutionary Algorithm. It uses a quality indicator, such as hypervolume contribution, directly as the fitness function for selection.

**SMSEMOA** [Beume *et al.*, 2007] The S-Metric Selection Evolutionary Multi-objective Algorithm is a steady-state algorithm, meaning only one individual is replaced in the population each generation. It uses the hypervolume indicator (S-metric) contribution to select which solution to discard. Typically, the algorithm removes the individual contributing the least hypervolume from the worst non-dominated front to make room for a new offspring.

**PESA2** [Corne *et al.*, 2001] The Pareto Envelope-based Selection Algorithm 2 introduces a region-based selection mechanism for MOEAs. Instead of assigning fitness to individual solutions, PESA2 partitions the *objective space* into hyperrectangles (regions) and assigns fitness to these regions based on the number of non-dominated solutions they contain in an external archive. A parent to mutate is then selected by first choosing a hyperrectangle that favors less crowded regions to promote diversity and then randomly selecting an individual from within that hyperrectangle.

**RNSGA-II** [Deb and Sundar, 2006] A variant of NSGA-II that incorporates reference points to guide the search and can be effective particularly for many-objective problems.

**UNSGA3** [Seada and Deb, 2016] The Unified Non-dominated Sorting Genetic Algorithm III can efficiently tackle single-, multi-, and many-objective optimization problems. It modifies the NSGA-III approach primarily through a niching-based tournament selection mechanism.

**CTAEA** [Li *et al.*, 2018] A *Two-Archive* algorithm that maintains one archive for convergence and another for diversity, aiming to balance the two explicitly.

## C Operational Costs and API Usage

In this section, we provide the API costs and providers for the LLMs used throughout the experiments in this paper. All costs are measured per million tokens and are based on the pricing as of the time of the experiments. The models were accessed through the following main providers: Google API<sup>6</sup>, Nebius AI<sup>7</sup> and OpenAI API<sup>8</sup>.

<sup>6</sup><https://cloud.google.com/apis>

<sup>7</sup><https://github.com/nebious/api>

<sup>8</sup><https://platform.openai.com/docs/api-reference>

Table 3: API cost structure for language models used in the experiments.

Model	Provider	Input Cost (per 1M tokens)	Output Cost (per 1M tokens)
Gemini-2.0-Flash	Google	\$0.10	\$0.40
Gemma-2-2B	Nebius	\$0.10	\$0.10
Gemma-2-9B	Nebius	\$0.10	\$0.10
GPT-4o-mini	OpenAI	\$0.15	\$0.60
GPT-OSS-120B	Nebius	\$0.60	\$0.60
LLaMA-3.1-8B	Nebius	\$0.10	\$0.10
LLaMA-3.3-70B	Nebius	\$0.60	\$0.60
Qwen3-32B	Nebius	\$0.60	\$0.60

In Table 4 we show the measured operational costs of MOHOLLM with different LLM models on the Vehicle-Safety benchmark. Gemini-2.0-Flash is the fastest model both per trial and overall, while LLaMA-3.1-8B achieves by far the lowest monetary cost. LLaMA-3.3-70B uses the fewest API requests and the lowest total tokens on average, but at higher runtime, whereas Qwen3-32B and GPT-OSS-120B have higher token usage, runtime, and cost.

## D Robustness and Instruction Adherence

In this section, we analyze the instruction-following abilities of the LLM when generating a candidate by quantifying the duplicate (identical to another solution generated within the same batch), reobservation (identical to a point already evaluated in a previous iteration) and out-of-region rate of its candidate generation process. In the experiments, whenever the LLM samples a out-of-region point, we rerun the generative process until it samples a candidate within the region.

In Table 5, we analyze the rejection rates of MOHOLLM with different LLM models on the VehicleSafety benchmark. Results indicate that LLMs sometimes struggle to respect hard numerical boundaries, a difficulty that is amplified at later iterations when the partitions become increasingly narrow. Within the LLaMA family, *LLaMA-3.1-8B* fails on over 50% of proposals, whereas the *70B* variant shows only 6% out-of-region rate. *GPT-OSS 120B* suffers a rejection rate of nearly 30%, significantly higher than the smaller LLaMA model. On the other hand, the smaller *Gemma-2-9B* demonstrates superior constraint adherence compared to the 8B LLaMA model, highlighting that architectural choices and training data composition are as important as parameter count for numerical reasoning tasks.

## E Additional Experimental Results

In this section, we present additional experimental results illustrating the performance of MOHOLLM across both synthetic and real-world benchmark problems, more analysis results and ablations.

Table 4: A comparison of operational costs for various language models. Results show the mean  $\pm$  standard error of 10 independent seeds on the VehicleSafety benchmark. The best performance (lowest value) for each metric is marked in **bold**.

Model	Gemini-2.0-Flash	LLaMA-3.3-70B	LLaMA-3.1-8B	Qwen3-32B	Gemma-2-9B	GPT-4o-mini	GPT-OSS-120B
<i>Average Per-Trial</i>							
Time (s)	<b>20.59 <math>\pm</math> 1.64</b>	70.01 $\pm$ 5.42	117.24 $\pm$ 24.74	224.12 $\pm$ 30.08	37.04 $\pm$ 6.37	58.53 $\pm$ 5.03	250.28 $\pm$ 51.33
Prompt Tokens	<b>44387 <math>\pm</math> 30286</b>	56792 $\pm$ 8656	114776 $\pm$ 7250	67263 $\pm$ 7898	91503 $\pm$ 15878	58357 $\pm$ 4037	92596 $\pm$ 25016
Completion Tokens	<b>2923 <math>\pm</math> 1872</b>	3435 $\pm$ 103	7651 $\pm$ 1256	70826 $\pm$ 8140	4497 $\pm$ 514	3581 $\pm$ 111	63615 $\pm$ 11490
Total Tokens	<b>47310 <math>\pm</math> 32139</b>	60227 $\pm$ 8756	122427 $\pm$ 8008	138089 $\pm$ 15868	96000 $\pm$ 16387	61938 $\pm$ 4119	156212 $\pm$ 34091
API Requests	21 $\pm$ 3.5	<b>20 <math>\pm</math> 2.2</b>	39 $\pm$ 2.2	22 $\pm$ 2.7	28 $\pm$ 4.4	21 $\pm$ 1.2	32 $\pm$ 8.9
Cost ( $\times 10^{-3}$ \$)	7.918 $\pm$ 0.760	8.757 $\pm$ 1.165	<b>2.755 <math>\pm</math> 0.197</b>	55.948 $\pm$ 6.413	3.150 $\pm$ 0.522	10.902 $\pm$ 0.656	52.059 $\pm$ 9.900
<i>Average Total</i>							
Tokens	933693 $\pm$ 223702	<b>722723 <math>\pm</math> 105074</b>	1469130 $\pm$ 96102	1657063 $\pm$ 190416	1151996 $\pm$ 196649	743253 $\pm$ 49430	1874542 $\pm$ 409092
Cost (\$)	0.10930 $\pm$ 0.02439	0.10508 $\pm$ 0.01398	<b>0.03306 <math>\pm</math> 0.00236</b>	0.67138 $\pm$ 0.07696	0.03780 $\pm$ 0.00627	0.13082 $\pm$ 0.00787	0.62470 $\pm$ 0.11879
Time (s)	<b>300.10 <math>\pm</math> 25.13</b>	857.72 $\pm$ 79.88	1444.58 $\pm$ 330.08	2689.42 $\pm$ 360.97	444.51 $\pm$ 76.49	702.42 $\pm$ 60.34	3003.39 $\pm$ 615.91

Table 5: Analysis of model efficiency and rejection rates on the VehicleSafety benchmark (mean over 10 seeds). **LLaMA-3.1-8B** exhibits the highest failure rate, rejecting over half of all generated proposals.

Model	Gemini-2.0-Flash	LLaMA-3.3-70B	LLaMA-3.1-8B	Qwen3-32B	Gemma-2-9B	GPT-4o-mini	GPT-OSS-120B
<b>Avg. Total Proposed</b>	<b>554.1</b>	556.7	1213.3	599.0	743.4	577.8	798.7
<i>Rejection Rate Breakdown (%)</i>							
Duplicate	0.08	<b>0.00</b>	0.89	<b>0.00</b>	<b>0.00</b>	<b>0.00</b>	<b>0.00</b>
Re-observed	1.01	0.12	1.49	<b>0.00</b>	0.01	<b>0.00</b>	1.49
Out of Region	<b>4.85</b>	6.09	49.28	11.69	29.50	8.08	27.18
<b>Total Rejection Rate</b>	<b>5.93</b>	6.21	51.66	11.69	29.52	8.08	28.67

Table 6: Per-objective surrogate prediction accuracy on the Car-SideImpact benchmark, reporting  $R^2$ , MSE, Kendall’s  $\tau$ , and Spearman’s  $\rho$  over  $N = 700$  test points for each method and objective.

Method	Obj	$R^2 \uparrow$	MSE $\downarrow$	$\tau \uparrow$	$\rho \uparrow$	N
Gemini 2.0 Flash	F1	<b>0.877</b>	<b>5.53</b>	<b>0.786</b>	<b>0.931</b>	700
	F2	<b>0.645</b>	<b>0.02</b>	<b>0.632</b>	<b>0.800</b>	700
	F3	<b>0.874</b>	<b>0.05</b>	<b>0.774</b>	<b>0.920</b>	700
	F4	<b>0.632</b>	<b>4.32</b>	<b>0.682</b>	<b>0.847</b>	700
GP	F1	0.010	43.35	0.781	0.802	700
	F2	-6889.585	376.37	-0.513	-0.628	700
	F3	-496.359	149.84	-0.421	-0.467	700
	F4	-21.427	281.44	-0.129	-0.155	700
TabPFN-v2	F1	-5.616	242.86	0.061	0.037	700
	F2	-3340.140	196.87	0.127	0.140	700
	F3	-287.800	88.74	0.116	0.140	700
	F4	-15.547	204.81	0.107	0.154	700

Table 7: Per-objective surrogate prediction accuracy on the Penicillin benchmark, reporting  $R^2$ , MSE, Kendall’s  $\tau$ , and Spearman’s  $\rho$  over  $N = 700$  test points for each method and objective.

Method	Obj	$R^2$	MSE	$\tau$	$\rho$	N
Gemini 2.0 Flash	F1	<b>0.742</b>	<b>8.06</b>	<b>0.684</b>	<b>0.851</b>	700
	F2	<b>0.792</b>	<b>122.67</b>	<b>0.797</b>	<b>0.896</b>	700
	F3	<b>0.787</b>	<b>6031.37</b>	<b>0.824</b>	<b>0.909</b>	700
GP	F1	-9.721	314.59	0.274	0.371	700
	F2	-0.769	1039.85	-0.210	-0.295	700
	F3	-0.397	39389.47	0.028	0.065	700
TabPFN-v2	F1	-173.697	5184.01	0.375	0.487	700
	F2	-0.537	987.24	0.392	0.475	700
	F3	0.491	11916.89	0.573	0.720	700

Table 8: Per-objective surrogate prediction accuracy on the VehicleSafety benchmark, reporting  $R^2$ , MSE, Kendall’s  $\tau$ , and Spearman’s  $\rho$  over  $N = 700$  test points for each method and objective.

Method	Obj	$R^2$	MSE	$\tau$	$\rho$	N
Gemini 2.0 Flash	F1	<b>0.806</b>	<b>7.57</b>	<b>0.758</b>	<b>0.903</b>	700
	F2	<b>0.655</b>	<b>0.25</b>	<b>0.672</b>	<b>0.805</b>	700
	F3	<b>0.524</b>	<b>0.00</b>	<b>0.655</b>	<b>0.813</b>	700
GP	F1	-9038.058	402521.05	0.709	0.719	700
	F2	-2671946.160	2216819.87	0.257	0.345	700
	F3	-1789516768.903	1952829.18	0.056	0.069	700
TabPFN-v2	F1	-16837.928	1272547.79	0.286	0.306	700
	F2	-1349159.150	1365562.21	0.221	0.274	700
	F3	-1273121958.222	1111401.55	0.190	0.234	700

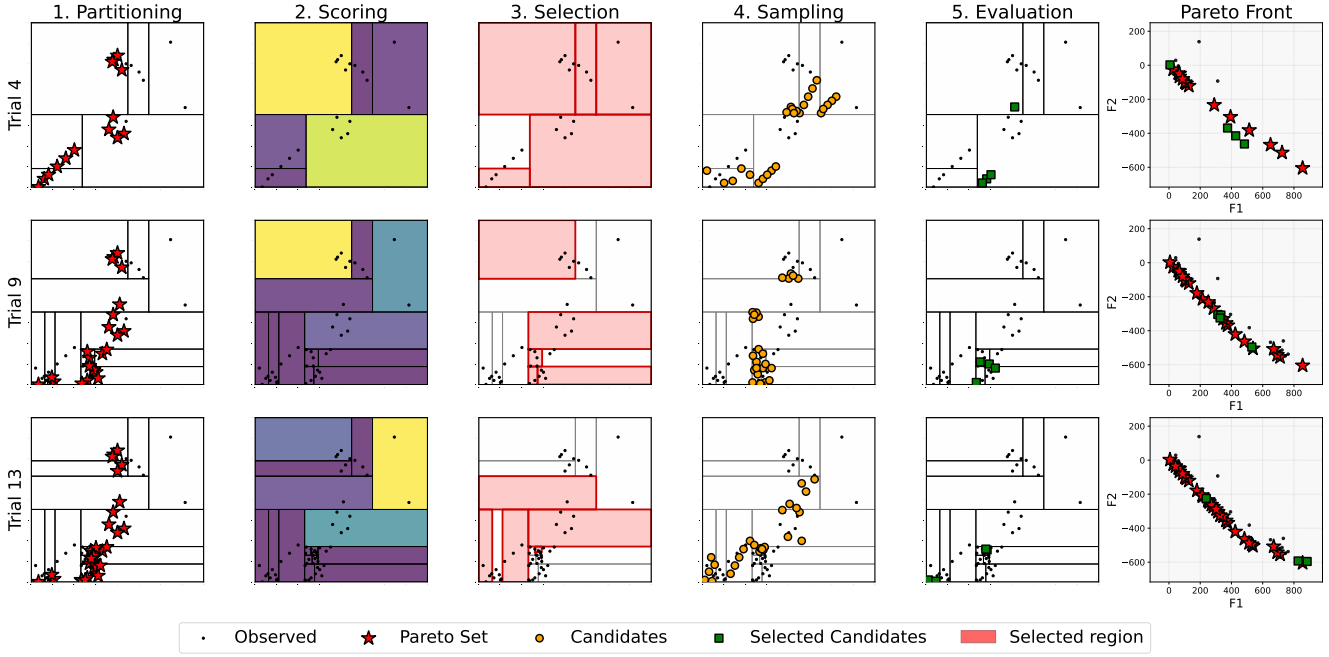


Figure 7: Search process of MOHOLLM on the 2D Chankong-Haines function at different optimization stages. The last column illustrates the function values, while other columns the five algorithmic steps: partitioning, region scoring, probabilistic selection, LLM-based sampling, and evaluation. Rows correspond to early, intermediate, and late trials. MOHOLLM transitions from coarse, globally exploratory partitions to fine-grained, localized refinement around the Pareto front, allocating samples to both sparse regions and dense Pareto-optimal areas.

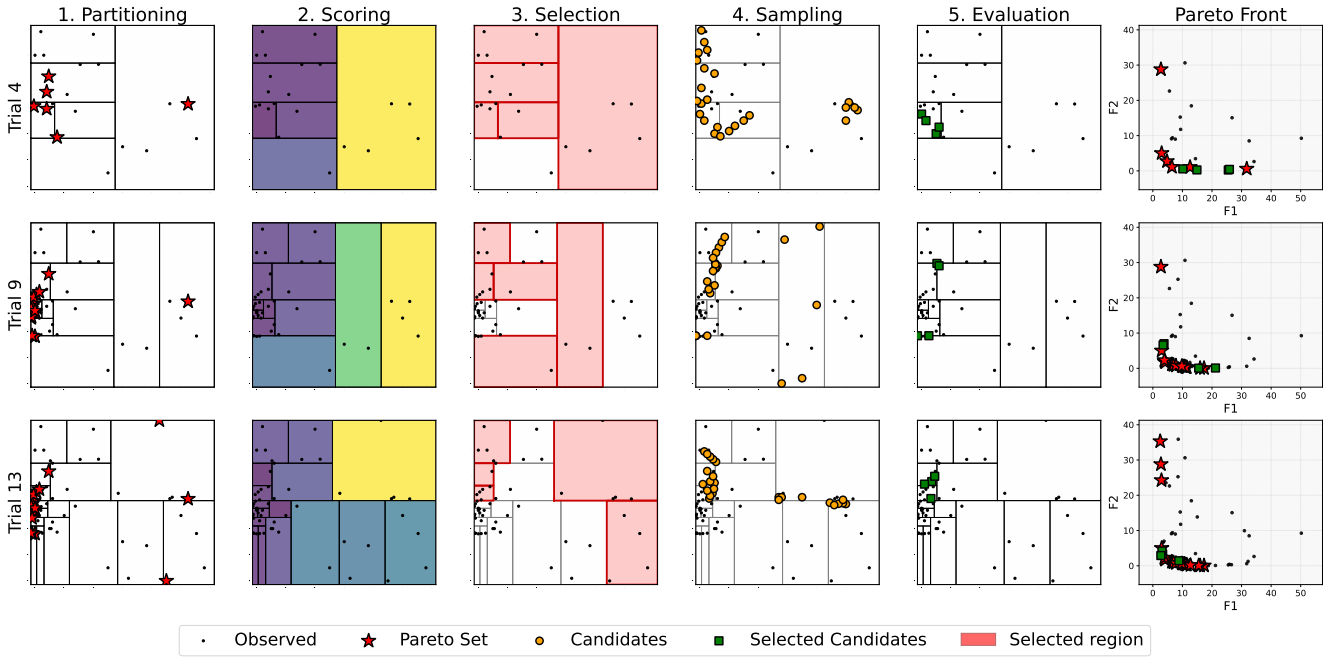


Figure 8: Search process of MOHOLLM on the 2D Poloni function at different optimization stages. The last column illustrates the function values, while other columns the five algorithmic steps: partitioning, region scoring, probabilistic selection, LLM-based sampling, and evaluation. Rows correspond to early, intermediate, and late trials. MOHOLLM transitions from coarse, globally exploratory partitions to fine-grained, localized refinement around the Pareto front, allocating samples to both sparse regions and dense Pareto-optimal areas.

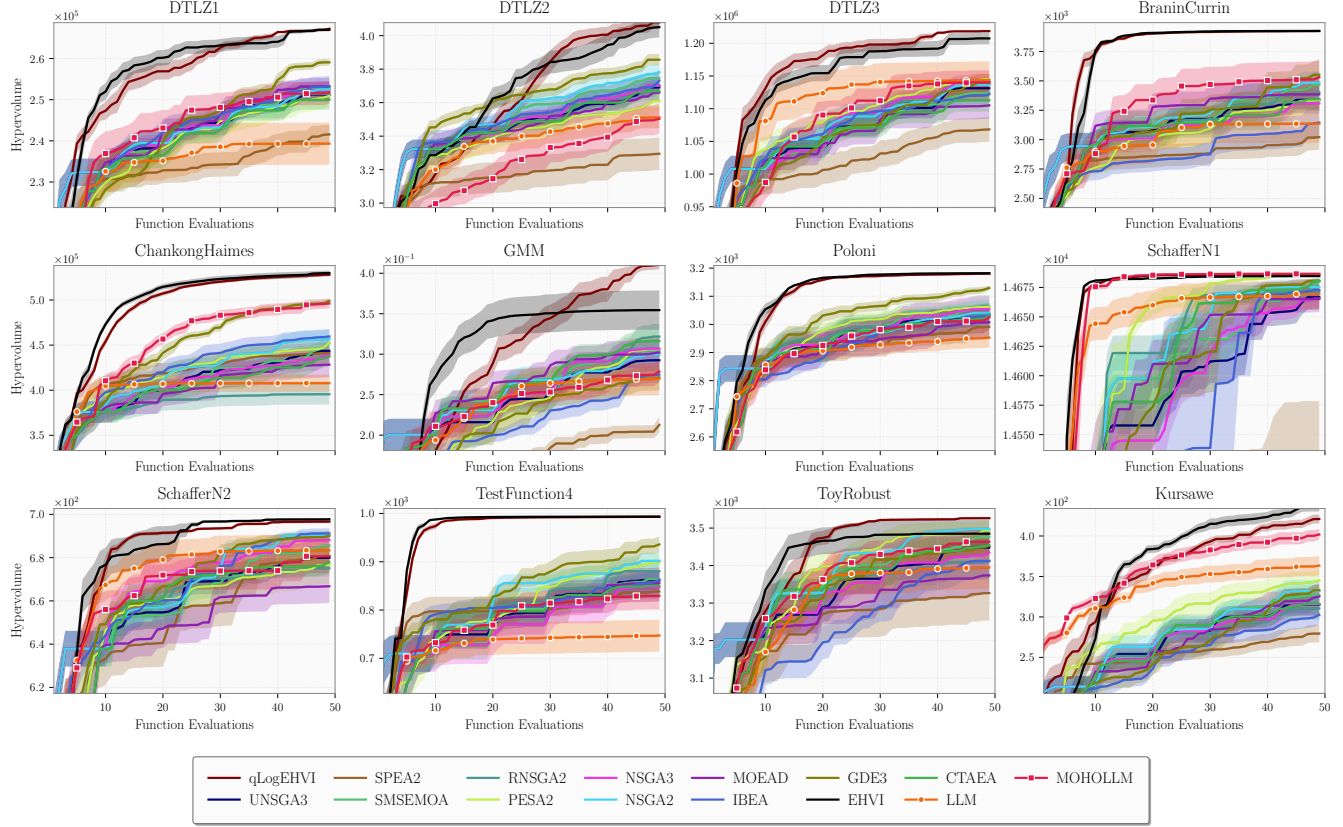


Figure 9: Hypervolume (HV) trajectory over function evaluations on the synthetic benchmark problems. Curves report the mean HV across 10 runs, and shaded regions indicating the 95% CI. MOHOLL shows competitive performance across all tasks, in contrast to the unconstrained LLM baseline, which rapidly stagnates.

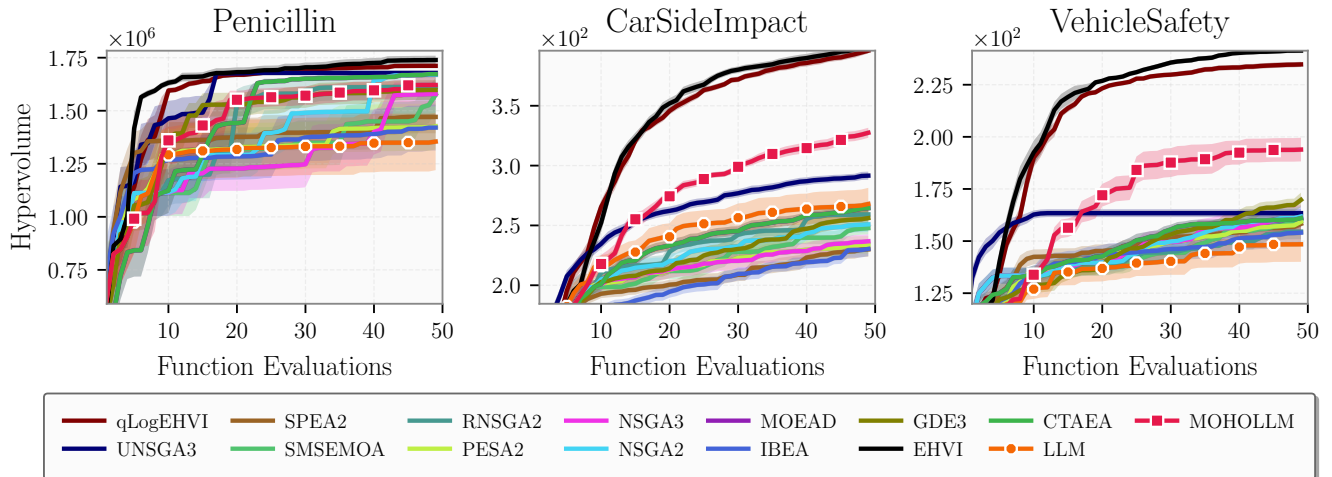


Figure 10: Hypervolume (HV) trajectory over function evaluations on real-world benchmarks (Penicillin, VehicleSafety, and CarSideImpact). Curves report the mean HV across 10 runs, and shaded regions indicating the 95% CI. MOHOLL shows competitive performance across all tasks, in contrast to the unconstrained LLM baseline, which rapidly stagnates..

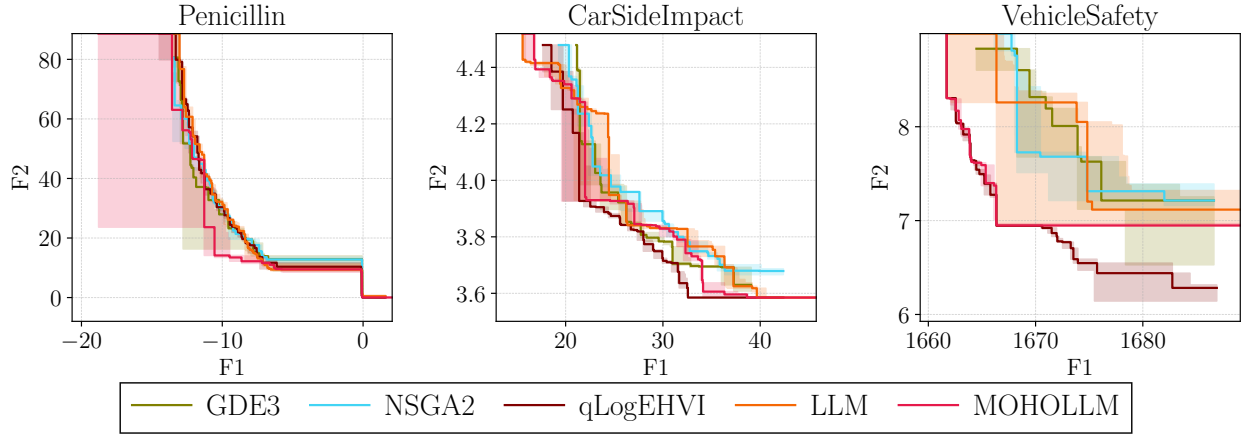


Figure 11: Empirical Attainment Function (EAF) on the real-world benchmarks (Penicillin, CarSideImpact, and VehicleSafety). For each problem, the plots show the EAF aggregated over 10 independent runs, comparing MOHOLLMM against representative baselines (GDE3, NSGA-II, qLogEHVI, and the global LLM). Shaded regions indicate the variance across runs.

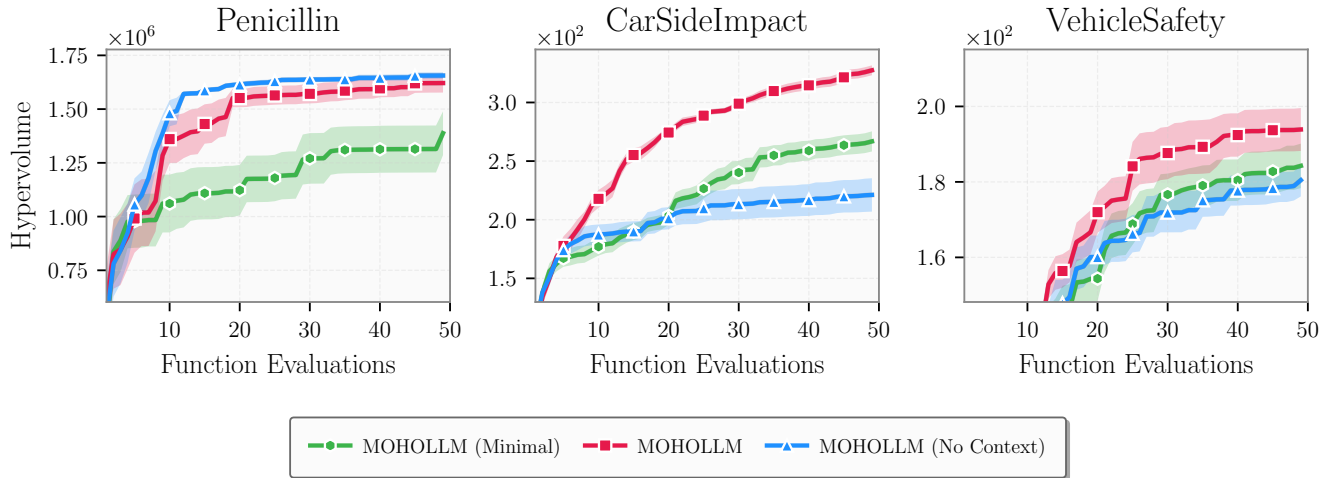


Figure 12: Prompt ablations on real-world benchmarks (Penicillin, VehicleSafety, and CarSideImpact). We compare the full MOHOLLMM configuration against variants obtained by removing or modifying prompt components.

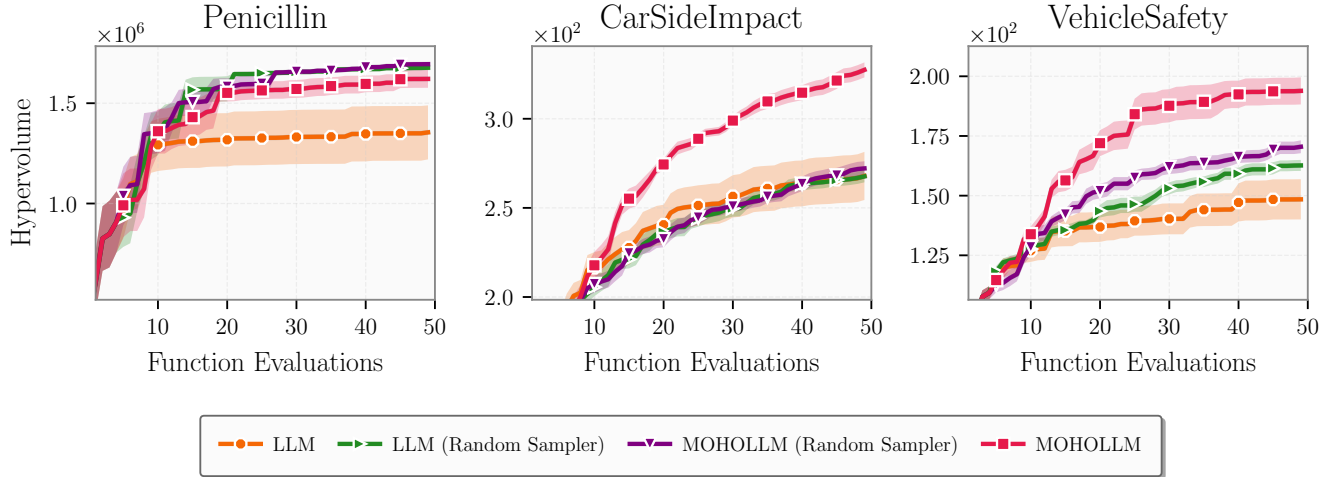


Figure 13: Candidate sampler ablation comparing MOHOLLMM against variants with a random candidate sampler.

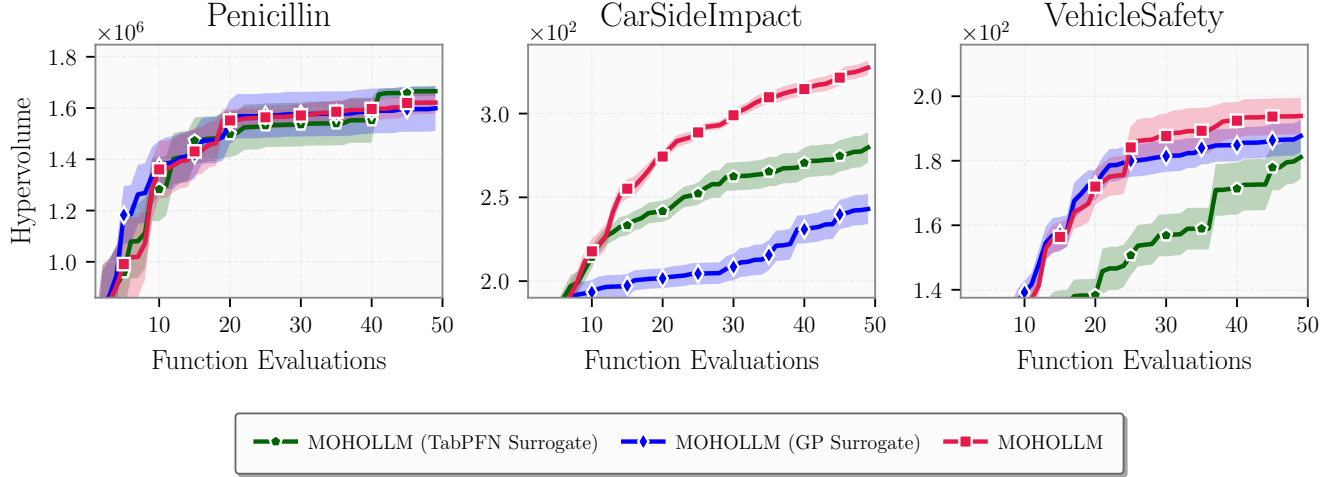


Figure 14: Surrogate model ablation on the real-world benchmarks (Penicillin, CarSideImpact, and VehicleSafety), comparing MOHOLLMM with different surrogate choices (TabPFN surrogate and GP surrogate) against the default LLM surrogate. We report the mean hypervolume trajectories over 10 runs with 95% confidence intervals.

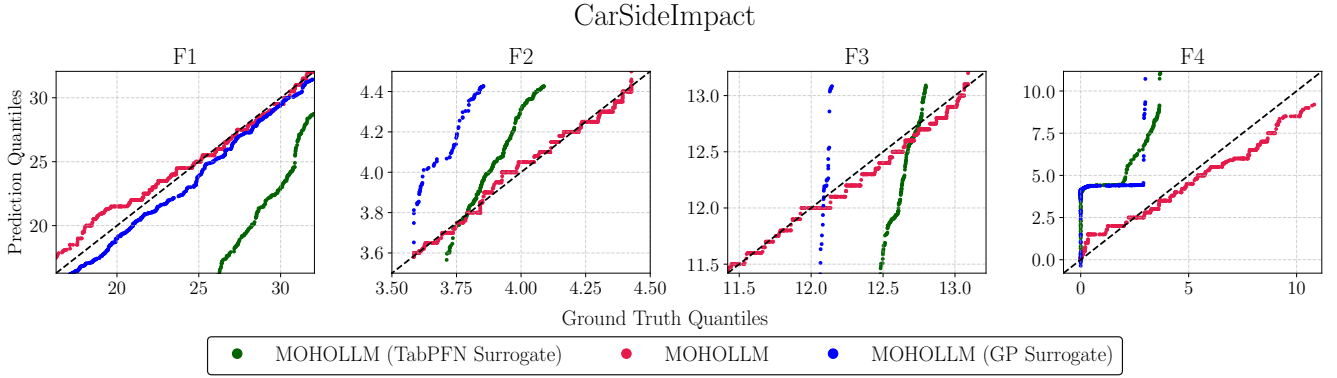


Figure 15: Q-Q plots on CarSideImpact comparing surrogate predictions against ground-truth quantiles for each objective (F1–F5), illustrating calibration and distributional alignment of the TabPFN, GP, and default LLM surrogates.

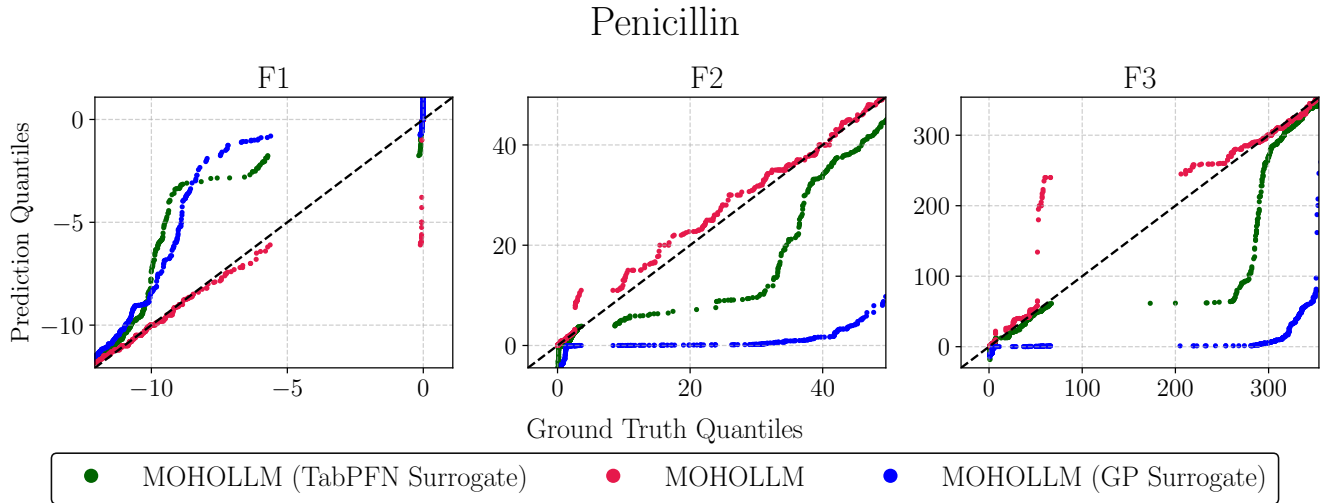


Figure 16: Q-Q plots on Penicillin analogue to Figure 15.

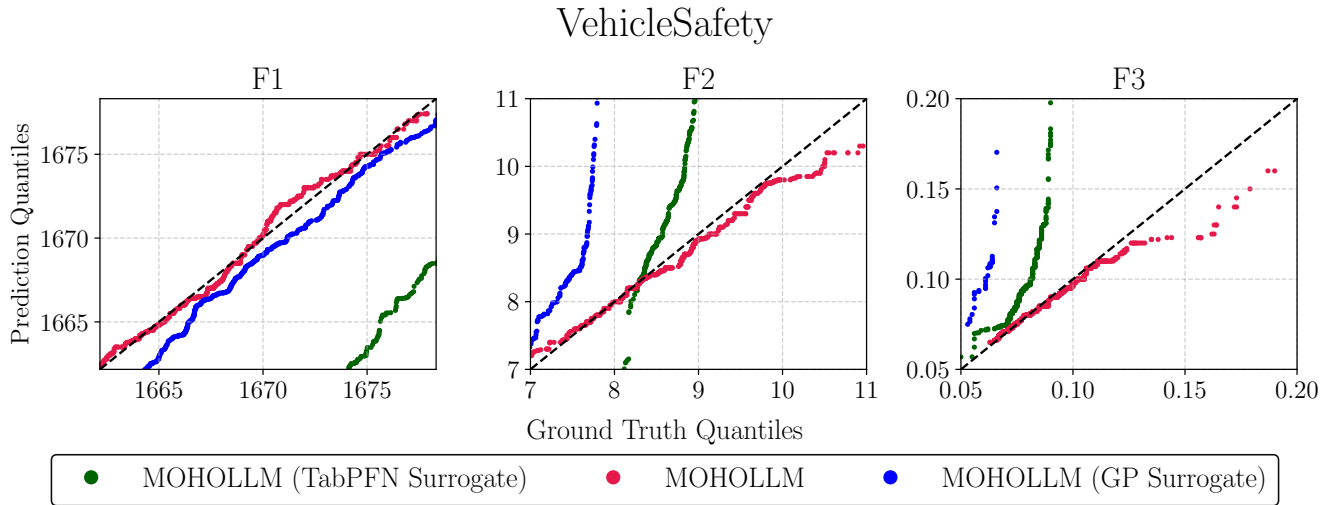


Figure 17: Q-Q plots on VehicleSafety analogue to Figure 15.

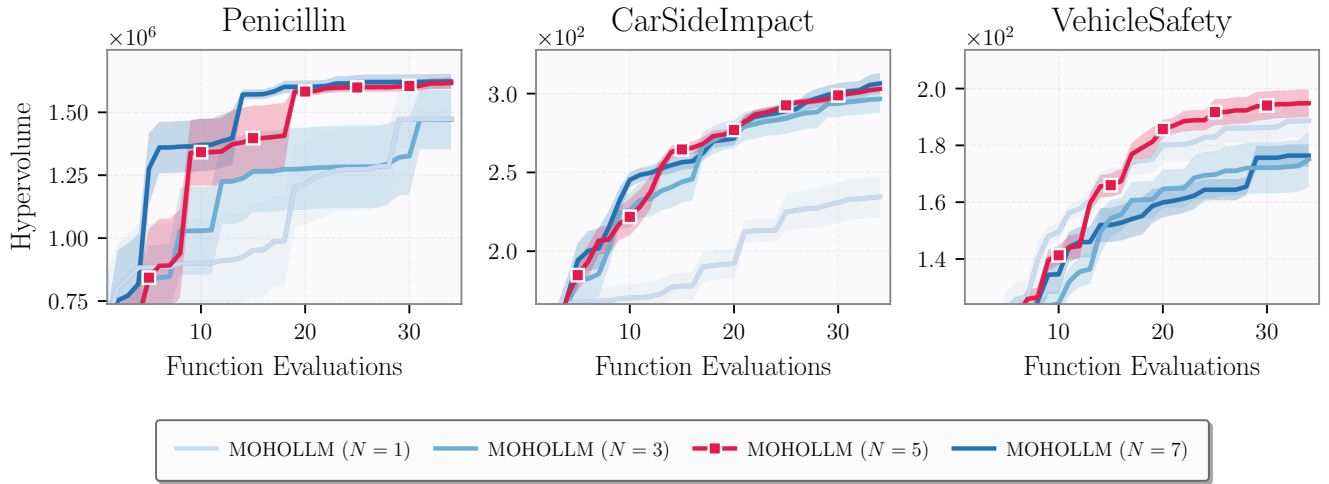


Figure 18: The effect of varying the number of candidates  $N$  generated from the LLM per iteration on the real-world benchmarks. Higher  $N$  typically improves convergence speed and final solution quality up to a saturation point.

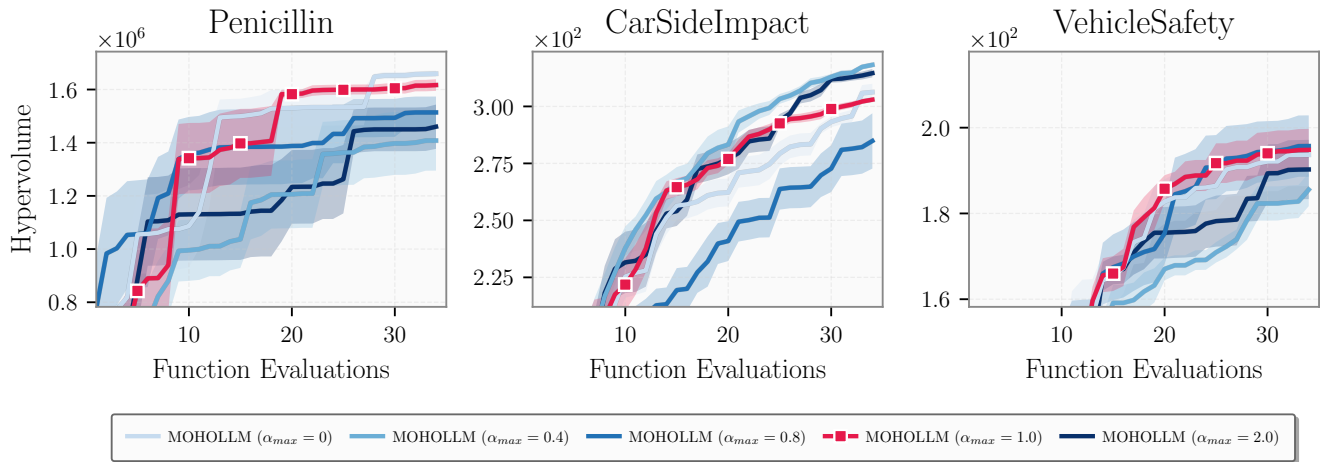


Figure 19: The effect of varying  $\alpha_{max}$  on the real-world benchmarks.

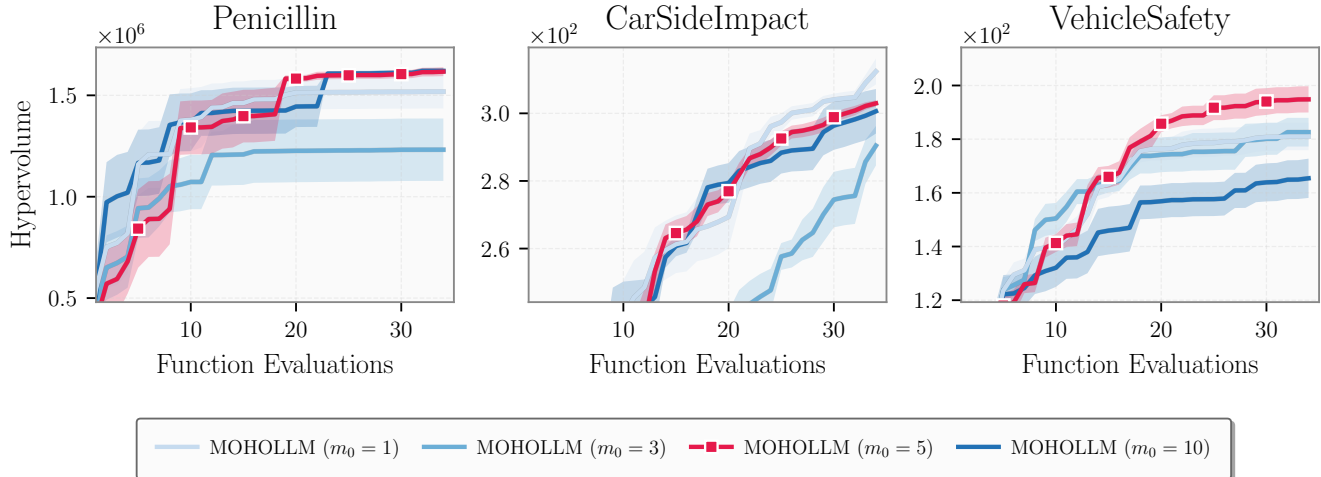


Figure 20: The effect of varying the initial maximum leaf size  $m_0$  on the real-world benchmarks.  $m_0 = 5$  is a robust choice.

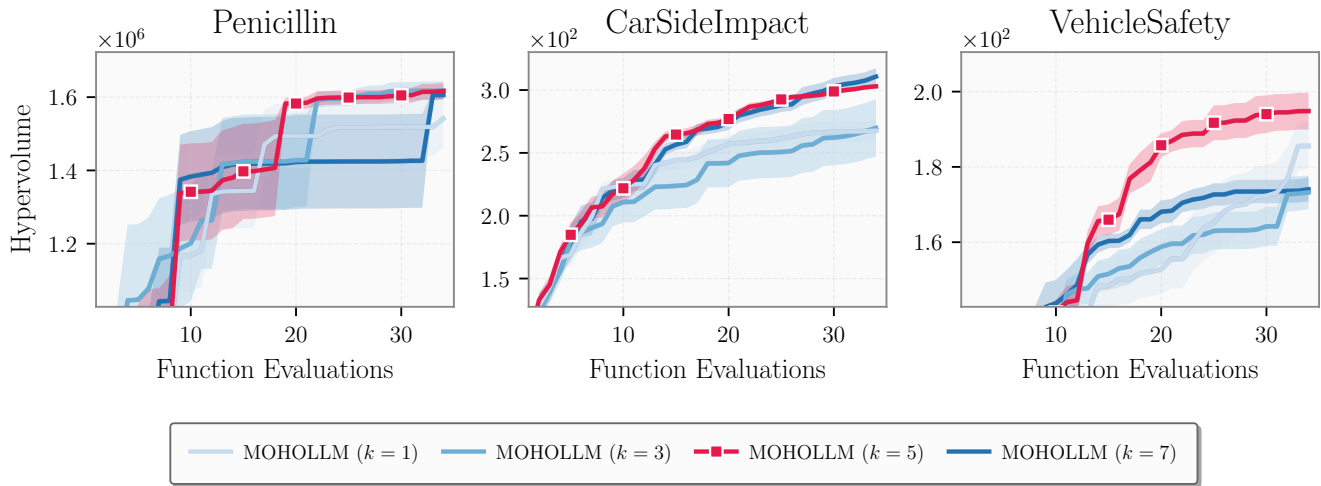


Figure 21: The effect of varying the number of sampled regions  $k$  on the real-world benchmarks.

Table 9: Definition of the dynamic prompt variables used in MOHOLLM.

Placeholder	Description	Example Content
<code>\$metrics</code>	The specific objective functions to be optimized.	F1 (lower is better), F2 (lower is better)
<code>\$region_constraints</code>	The hard bounds of the current hyper-rectangular partition (leaf node).	<code>{lr: range(float([0.0, 0.9])), num_layer: range(int([1, 20]))}</code>
<code>\$region_ICL_examples</code>	In-Context Learning examples sampled from the history $\mathcal{D}_t$ to guide generation.	<code>{lr: 0.4, num_layer: 8}</code> F1: 5.65
<code>\$target_number_of_candidates</code>	The number of candidates ( $M$ ) requested from the sampler.	15
<code>\$candidate_sampler_response_format</code>	The required JSON schema for output parsing.	<code>{lr: float, num_layer: int}</code>
<code>\$target_architectures</code>	The set of newly generated candidates requiring surrogate scoring.	1: <code>{lr: 0.4, ...}</code> 2: <code>{lr: 0.03, ...}</code>
<code>\$surrogate_model_response_format</code>	The required JSON schema for predicted values.	<code>{F1: float, F2: float}</code>

## F Prompt Engineering and Templates

### F.1 Generic Prompt Templates

To enable the LLM to act as both a candidate sampler and a surrogate model, we employ structured prompt templates. These templates are dynamically populated at each iteration with task-specific constraints, optimization history, and performance metrics. We visually distinguish the templates by function: **blue** for candidate sampling and **green** for surrogate modeling. Listing 1 and 2 present the main templates.

```
# Optimization task

## Problem Description
You are tasked with solving a optimization problem that
requires finding optimal solutions.

- **Evaluation**: Configurations are measured by $metrics

$description

## Constraints
The allowable ranges for the hyperparameters are:
$input_boundaries

## Previously Evaluated configurations
Below are examples of configurations that have been
evaluated, showing their operations and performance
metrics:

$ICL_examples

## Your Task
Generate $target_number_of_candidates new configurations
that:
1. Are likely to achieve lower $metrics than the examples
2. Are different from all previously evaluated
   configurations
3. Satisfy all the specified constraints:
   $input_boundaries

## Output Format
Each configuration has to follow this format:

$candidate_sampler_response_format

Provide your response in a JSON list containing each
proposed configuration.
Return only the required JSON list output without
additional text.
```

Listing 1: Generic prompt template for the candidate sampler.

```
$target_architectures

## Your Task
1. Predict the $metrics value for each candidate
   configuration
2. Base your predictions on patterns in the reference
   examples

## Output Format
Each evaluation has to follow this format:

$surrogate_model_response_format

Provide your response in a JSON list containing each
proposed evaluation.
Return only the required JSON list output without
additional text.
```

Listing 2: Generic prompt template for the surrogate Model.

### F.2 Prompt Variable Definitions

Table 9 details the dynamic placeholders used within the templates. These tags are programmatically replaced at runtime based on the current leaf regions' boundaries and the optimization history.

### F.3 Prompt Ablation Studies

The following listings shows the Minimal templates used to isolate the impact of prompt complexity.

```
Previously Evaluated Configurations:
$Region_ICL_examples

Generate $target_number_of_candidates new configurations
that:
1. Are likely to achieve lower $metrics than the examples
2. Are different from all previously evaluated
   configurations
3. Satisfy all the specified constraints:
   $region_constraints

Format:
Each configuration has to follow this format:

$candidate_sampler_response_format

Provide your response in a JSON list containing each
proposed configuration.
Return only the required JSON list output without
additional text.
```

Listing 3: Minimal candidate sampler prompt template (ablation).

```
# Configuration Performance Prediction

## Problem Description
You are tasked with predicting the performance of
configurations.

- **Evaluation Metric**: $metrics (to be predicted)
- **Constraint**: The allowable ranges for the
   hyperparameter are: $input_boundaries

$description

## Reference configurations with Known Performance
Below are examples of configurations that have been
evaluated, showing their operations and performance
metrics:

$ICL_examples

## Candidate configurations to Evaluate
You must predict performance for these new configurations:
```

```
Previously Evaluated Configurations:
$Region_ICL_examples

Predict performance for these configurations:
$target_architectures

Task:
1. Predict the $metrics value for each candidate
   configuration
2. Base your predictions on patterns in the reference
   examples

Format:
Each evaluation has to follow this format:

$surrogate_model_response_format
```

Provide your response in a JSON list containing each proposed evaluation.  
Return only the required JSON list output without additional text.

Listing 4: Minimal surrogate prompt template (ablation).

#### F.4 Domain-Specific Contexts

For real-world benchmarks, we inject specific problem descriptions into the `$description` tag to aid the LLM's semantic reasoning.

Your task is to optimize the design of a vehicle for frontal crash safety by adjusting the material thickness of five key structural components. You will generate a configuration for:  $x_0$ , the bumper beam that absorbs initial impact;  $x_1$ , the crash box designed to crush progressively;  $x_2$ , the main longitudinal rails that channel energy;  $x_3$ , the A-pillar that protects the cabin integrity; and  $x_4$ , the dash panel that prevents intrusion into the legroom area. The performance of your design will be evaluated against three competing objectives to be minimized:  $F_1$  is the total vehicle mass,  $F_2$  is the chest injury criterion, and  $F_3$  is the toe board intrusion. Your goal is to propose designs that find the best trade-off between minimizing weight, occupant injury, and structural deformation.

Listing 5: Context for the VehicleSafety benchmark.

Your task is to propose optimal designs for a vehicle to improve its safety in a side-impact collision. You will generate a configuration of seven input variables representing the thickness of key structural components:  $x_0$  (B-Pillar inner),  $x_1$  (B-Pillar reinforcement),  $x_2$  (floor side inner),  $x_3$  (cross-member),  $x_4$  (door beam),  $x_5$  (door beltline reinforcement), and  $x_6$  (roof rail). The performance of your design will be judged on four objectives, all of which should be minimized:  $F_1$  is the vehicle's total weight,  $F_2$  is the injury load on the occupant's abdomen,  $F_3$  is the intrusion velocity at key points, and  $F_4$  is a penalty for any constraint violations. Your goal is to find designs that represent the best possible trade-offs across these competing safety and engineering metrics.

Listing 6: Context for the CarSideImpact benchmark.

Your task is to find the optimal settings for a simulated fed-batch penicillin production process. You will generate a configuration of seven input control parameters that define the initial conditions and operation of the fermenter. These parameters are:  $x_0$ , the culture medium volume;  $x_1$ , the biomass concentration;  $x_2$ , the operating temperature;  $x_3$ , the glucose substrate concentration;  $x_4$ , the substrate feed rate;  $x_5$ , the substrate feed concentration; and  $x_6$ , the  $H^+$  concentration (acidity). The success of your configuration is evaluated on three metrics in a multi-objective optimization context, all of which are to be minimized.  $F_1$  represents the negative final penicillin yield,  $F_2$  is the total production time, and  $F_3$  is the total  $CO_2$  emission byproduct. Your goal is to propose configurations that find the best trade-offs by minimizing all three competing objectives.

Listing 7: Context for the Penicillin benchmark.

#### F.5 Instantiated Examples (Poloni Benchmark)

To illustrate how the templates are populated during runtime, the following listings show the exact prompts sent to the LLM for the *Poloni* benchmark.

```

# Optimization task
## Problem Description
You are tasked with solving a optimization problem that
requires finding optimal solutions.

- **Evaluation**: Configurations are measured by  $F_1$  (lower
  is better),  $F_2$  (lower is better)

## Constraints
The allowable ranges for the hyperparameters are:
{
  x: range(float([-3.142, -1.067])),
  y: range(float([0.274, 3.142]))
}

## Previously Evaluated Configurations
Below are examples of configurations that have been
evaluated, showing their operations and performance
metrics:

Configuration: {"x": -3.142, "y": -0.725}
F1: 13.327, F2: 0.096

Configuration: {"x": -3.142, "y": -0.706}
F1: 13.178, F2: 0.107

Configuration: {"x": -3.142, "y": -0.162}
F1: 7.839, F2: 0.722

Configuration: {"x": 0.975, "y": 1.681}
F1: 1.18, F2: 22.988

Configuration: {"x": -3.142, "y": -0.82}
F1: 14.006, F2: 0.053

Configuration: {"x": -3.142, "y": 0.494}
F1: 2.616, F2: 2.252

Configuration: {"x": -3.142, "y": 0.017}
F1: 6.028, F2: 1.054

Configuration: {"x": -3.142, "y": -0.231}
F1: 8.566, F2: 0.612

Configuration: {"x": -3.142, "y": -0.392}
F1: 10.257, F2: 0.39

## Your Task
Generate 5 new configurations that:
1. Are likely to achieve lower  $F_1$  (lower is better),  $F_2$  (
  lower is better) than the examples
2. Are different from all previously evaluated
  configurations
3. Satisfy all the specified constraints: {
  x: range(float([-3.142, -1.067])),
  y: range(float([0.274, 3.142]))
}

## Output Format
Each configuration has to follow this format:
{"x": $x, "y": $y}

Provide your response in a JSON list containing each
proposed configuration.
Return only the required JSON list output without
additional text.

```

Listing 8: Example candidate sampler prompt used in the Poloni benchmark.

```

# Configuration Performance Prediction
## Problem Description
You are tasked with predicting the performance of
configurations.

- **Evaluation Metric**: F1 (lower is better), F2 (lower
is better) (to be predicted)

## Reference configurations with Known Performance
Below are examples of configurations that have been
evaluated, showing their operations and performance
metrics:

Configuration: {"x": -3.142, "y": -0.725}
F1: 13.327, F2: 0.096

Configuration: {"x": -3.142, "y": -0.706}
F1: 13.178, F2: 0.107

Configuration: {"x": -3.142, "y": -0.162}
F1: 7.839, F2: 0.722

Configuration: {"x": 0.975, "y": 1.681}
F1: 1.18, F2: 22.988

Configuration: {"x": -3.142, "y": -0.82}
F1: 14.006, F2: 0.053

Configuration: {"x": -3.142, "y": 0.494}
F1: 2.616, F2: 2.252

Configuration: {"x": -3.142, "y": 0.017}
F1: 6.028, F2: 1.054

Configuration: {"x": -3.142, "y": -0.231}
F1: 8.566, F2: 0.612

Configuration: {"x": -3.142, "y": -0.392}
F1: 10.257, F2: 0.39

## Candidate configurations to Evaluate
You must predict performance for these new configurations:

1: {"x": -2.742, "y": 0.474}
2: {"x": -2.342, "y": 0.674}
3: {"x": -2.542, "y": 0.574}
4: {"x": -2.942, "y": 0.374}
5: {"x": -2.142, "y": 0.774}

## Your Task
1. Predict the F1 (lower is better), F2 (lower is better)
value for each candidate configuration
2. Base your predictions on patterns in the reference
examples

## Output Format
Each evaluation has to follow this format:

{"F1": $F1, "F2": $F2}

Provide your response in a JSON list containing each
proposed evaluation.
Return only the required JSON list output without
additional text.

```

Listing 9: Example surrogate model prompt used in the Poloni benchmark.